CHAPTER IV

RESULTS AND DISCUSSION

A. Experimental Design: effects of spray-drying factors on production yields and moisture content

Spray drying was a method where the result strongly depended upon the material properties (BÜCHI Labortechnik AG, 1997). Thus, the instrument settings were in a combined system influencing the product properties. Experimental fractional factorial design was initially built to investigate the influence of factors on production yield and moisture content of spray-dried products. In this study, two processing parameters (inlet temperature, feed rate) and three formulation parameters (%solid content, %additive and polymer/extract ratio) were focused. Then, the optimal operating conditions were estimated by response surface methodology. Central rotational composite design was used to locate the experimental range containing the optimum for both maximizing production yield and minimizing moisture content.

1. Screening design: fractional factorial design (FFD)

The first step, values of the 19 runs from fractional factorial design 2^{5-1} (16 runs) with three center points (3 runs) were observed. The percentage yields and %moisture contents are shown in Table 5. The products were collected from the collector and cyclone, the amounts of the products from two sources were calculated as the percentage yields and the moisture contents were measured. The percentage yields varied from 27.92-47.50%. In parallel, the moisture contents varied from 4.18-13.92%. In some experiments, the operating conditions fixed by the experimental design resulted in promoting excessive sticking in the drying chamber. The resulting spray-dried products could not be collected and resulted to low percentage yields. Values of 19 run were computed with Design-Expert version 7.0.3 statistical software.

Table 5 Fractional factorial design matrix of five parameters and the observed responses

Code	Parameters					Responses			
	Inlet temp (° C)	Feed rate (ml/min)	Solid content (%)	Aerosil (%w/v)	Polymer /extract ratio	Yield (%)			Moisture content (%)
						cyclone	collector	total	
F1	(-) 140	(-) 5	(-) 2%	(-) 0%	(+)1.5/1	27.97	11.56	39.53	6.58 ±0.33
F2	(+) 160	(-) 5	(-) 2%	(-) 0%	(-)1/1	26.26	9.30	35.56	4.18 ±0.10
F3	(-) 140	(+) 7	(-) 2%	(-) 0%	(-)1/1	38.60	8.90	47.50	10.73 ±0.72
F4	(+) 160	(+) 7	(-) 2%	(-) 0%	(+)1.5/1	32.20	3.95	36.15	6.39 ±0.43
F5	(-) 140	(-) 5	(+) 4%	(-) 0%	(-)1/1	16.75	20.12	36.87	5.86 ±0.08
F6	(+) 160	(-) 5	(+) 4%	(-) 0%	(+)1.5/1	29.05	6.78	35.83	6.90 ±0.05
F7	(-) 140	(+) 7	(+) 4%	(-) 0%	(+)1.5/1	30.33	1.93	32.26	13.92 ±0.22
F8	(+) 160	(+) 7	(+) 4%	(-) 0%	(-)1/1	24.85	8.76	33.61	6.45 ±0.02
F9	(-) 140	(-) 5	(-) 2%	(+) 0.5%	(-)1/1	2.10	36.49	38.59	9.24 ±0.32
F10	(+) 160	(-) 5	(-) 2%	(+) 0.5%	(+)1.5/1	0.70	36.22	36.92	11.14 ±0.19
F11	(-) 140	(+) 7	(-) 2%	(+) 0.5%	(+)1.5/1	1.79	41.87	43.66	12.00 ±0.83
F12	(+) 160	(+) 7	(-) 2%	(+) 0.5%	(-)1/1	0.78	39.51	40.29	10.02 ±0.27
F13	(-) 140	(-) 5	(+) 4%	(+) 0.5%	(+)1.5/1	1.49	35.32	36.81	10.41 ±0.19
F14	(+) 160	(-) 5	(+) 4%	(+) 0.5%	(-)1/1	12.66	22.92	35.58	6.26 ±0.14
F15	(-) 140	(+) 7	(+) 4%	(+) 0.5%	(-)1/1	1.77	38.56	40.33	11.61 ±0.60
F16	(+) 160	(+) 7	(+) 4%	(+) 0.5%	(+)1.5/1	1.19	30.87	32.06	8.32 ±0.18
F17	(0) 150	(0) 6	(0) 3%	(0) 0.25%	(0)1.25/1	3.99	24.89	28.88	12.88 ±0.05
F18	(0) 150	(0) 6	(0) 3%	(0) 0.25%	(0)1.25/1	4.06	23.86	27.92	13.87 ±0.13
F19	(0) 150	(0) 6	(0) 3%	(0) 0.25%	(0)1.25/1	4.33	24.84	29.17	13.54 ±0.12

The analysis of variance (ANOVA) is required to test the significance and adequacy of the model. The Fisher variance ratio, F-value which is a statistically valid measure of how well the factors describe the variation in the data about its mean, could be calculated from ANOVA by dividing the mean square due to model variance by that due to error variance ($F_{model} = S_r^2 / S_e^2$). The greater the F-value is from unity, the more certain it is that the factors explain adequately the variation in the data about its mean, and the estimated factor effects were real.

In this step, the analysis of variance of the regression models demonstrated that the models were highly significant, as were evidenced from the Fisher's F-test (%yield: F_{model} = 65.24 and %moisture content: F_{model} = 41.73) and a low probability values (%yield: $P_{model} > F$ = 0.015 and %moisture content: $P_{model} > F$ = 0.024) (Table 6 and Table 7). Values of "Prob > F" were less than 0.05 indicated that model terms were significant ($P < 0.05$) (Montgomery, 2001).

The goodness of fit of the models was checked by the determination coefficients (R^2). The R^2 values provided a measure how much variability in the observed response values could be explained by the experimental factors and their interactions. The R^2 values are always between 0 and 1. The closer the R^2 values is to 1, the stronger the model be and the better it predicted the response. When expressed as a percentage, R^2 is interpreted as the percent variability in the response explained by the statistical model (Montgomery, 2001).

In this step, the values of R^2 = 0.9981 and 0.9970, indicated that 99.81% and 99.70% of variability in the response could be explained by the model for %yield and %moisture content, respectively (Table 6 and Table 7).

Table 6 ANOVA for selected factorial model of %yield

Source	Sum of squares	df	Mean square	*F*-value	Probability *P* (> *F*)
Model	446.790	16	27.920	65.240	0.015**
A-inlet temp	55.800	1	55.800	130.370	0.008*
B-feed	6.050	1	6.050	14.140	0.064
C-%solid	74.480	1	74.480	174.000	0.006*
D-%additive	3.290	1	3.290	7.700	0.109
E-ratio	13.650	1	13.650	31.900	0.030
AB	11.220	1	11.220	26.220	0.036
AC	7.340	1	7.340	17.160	0.054
AD	0.001	1	0.001	0.003	0.962
AE	2.740	1	2.740	6.400	0.127
BC	36.480	1	36.480	85.230	0.012
BD	2.540	1	2.540	5.940	0.135
BE	26.060	1	26.060	60.890	0.016
CD	2.120	1	2.120	4.950	0.156
CE	0.730	1	0.730	1.710	0.321
DE	1.420	1	1.420	3.310	0.211
Pure Error	0.860	2	0.430		
Corrected Total	447.640	18			

* Significant at *P value* = 0.01
** Significant at *P value* = 0.05
*** R-Squared = 0.9981

Table 7 ANOVA for selected factorial model of %moisture content

Source	Sum of squares	df	Mean square	*F*-value	Probability *P* (> *F*)
Model	169.650	16	10.600	41.730	0.024**
A-inlet temp	26.650	1	26.650	104.890	0.009*
B-feed	22.350	1	22.350	87.950	0.011
C-%solid	0.020	1	0.020	0.080	0.804
D-%additive	20.180	1	20.180	79.430	0.012
E-ratio	7.940	1	7.940	31.240	0.031
AB	11.410	1	11.410	44.890	0.022
AC	3.090	1	3.090	12.160	0.073
AD	2.010	1	2.010	7.910	0.107
AE	0.011	1	0.011	0.041	0.858
BC	0.520	1	0.520	2.050	0.288
BD	5.120	1	5.120	20.150	0.046
BE	3.640	1	3.640	14.320	0.063
CD	7.690	1	7.690	30.250	0.032
CE	3.430	1	3.430	13.510	0.067
DE	0.210	1	0.210	0.840	0.456
Pure Error	0.5100	2	0.2500		
Corrected Total	170.1500	18			

* Significant at *P value* = 0.01
** Significant at *P value* = 0.05
*** R-Squared = 0.9970

The *P*-values are used as a tool to check the significance of each of the coefficients which, in turn, are necessary to understand the pattern of the mutual interactions between the test variables. This implied that, result of %yield, the first order main effects of inlet temperature and %solid content were highly significant as were evident from their *P*-values = 0.008 and 0.006, respectively, so they were the most significant effects ($P < 0.01$) (Table 6). For result of %moisture content, the first order main effect of inlet temperature was a significant effect as was evident from its *P*-value = 0.009 ($P < 0.01$) (Table 7).

The coefficients of regression equations linking the responses to the experimental variables and interactions are indicated in Table 8.

Table 8 Coefficients of the regression equation linking the responses to the experimental factors and major interactions (coded units)

Parameters	**Coefficients**	
	%Yield	**%Moisture content**
Intercept	28.66	13.43
A-inlet temp	-1.87	-1.29
B-feed	0.61	1.18
C-%solid	-2.16	-0.04
D-%additive	0.45	1.12
E-ratio	-0.92	0.70
AB	-0.84	-0.84
AC	0.68	-0.44
AD	0.01	0.35
AE	0.41	0.03
BC	-1.51	0.18
BD	0.40	-0.57
BE	-1.28	-0.48
CD	0.36	-0.69
CE	-0.21	0.46
DE	0.30	-0.12

Main effects plots showed that the %yield could be considerably increased by reducing %solid content and inlet temperature. In addition, moisture content was reduced by increasing inlet temperature (Figure 18).

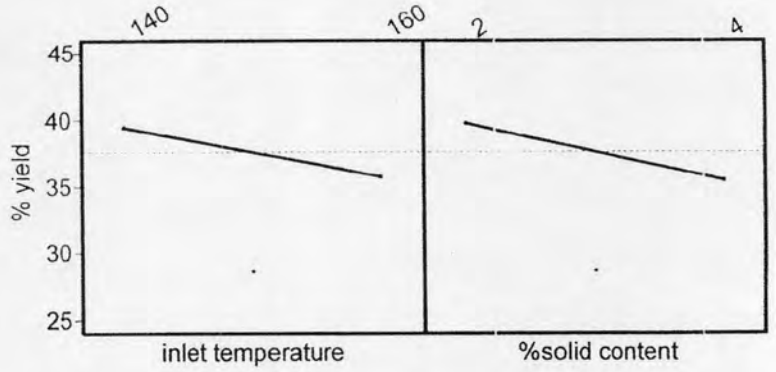

(a)

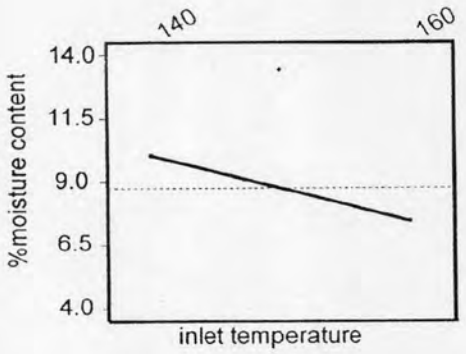

(b)

Figure 18 Main effect plots for % yield and %moisture content (factorial design);
(a) main effect plots of %yield, (b) main effect plot of %moisture content

The decrease of %solid content significantly improved the percentage yield (Figure 18a). It could be explained by the viscosity of spray solution was greatly influenced by %solid content (Table 35, appendix B). At high %solid content showed high viscosity value. The high viscosity of the spray solutions resulted in excessive sticking in the drying chamber and consequently, low yields.

A decreasing inlet temperature could improve percentage yield (Figure 18a). The reason of this finding was not clearly understood. It might be explained in regarding to the moisture content of the products. As decreasing the inlet temperature, the moisture content of the product increased and the high yield concurrently occurred.

This result disagreed with the previous study of spray drying of β-galactosidase. The percentage yield was improved with increased inlet temperature and decreased feed rate. The highest yield was obtained for the batch with the lowest moisture content (Broadhead, 1994).

Increased inlet air temperature resulted in decreased moisture content (Figure 18b). It could be explained by increased supplies of heat energy allowed a more efficient drying. This result agreed with a previous study by Labrude et al. (1989) that spray drying oxyhemoglobin.

It was observed that high moisture contents were related to with low outlet temperatures (Figure 19). The outlet temperature was the resulting temperature of the heat and mass balance in the drying chamber and thus could not be regulated. Due to the intense heat, mass transfer and the loss of humidity, the particles could be regarded to have the same temperature as the air. Thus, as a rule of thumb was: outlet temperature = maximum product temperature (BÜCHI Labortechnik AG, 1997).

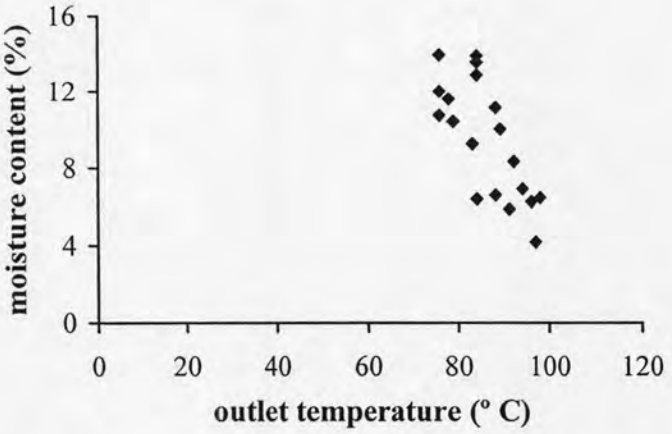

Figure 19 A scattered plot between outlet temperature and moisture content on spray-dried microspheres

In this study a diminution of outlet temperature indicated that the thermal energy supplied by range of inlet temperatures used, was not sufficient to allow complete drying. Additionally, a range of feed rates used in this study was limited in a narrow range and too high (5-7 ml/min). So, the higher energy supply was needed and might be reason for feed rate was also no significant effect for responses. In these cases, sticking occurred in the drying chamber and represented with high moisture content.

However, this result was not relevant with the previous study in that the optimum inlet temperature for the preparation of chitosan microspheres from aqueous solutions of chitosan was found to be 160°C. If the inlet temperature was set below 140°C, or the pump rate was chosen to be faster than 10 ml/min, the solvent in the droplets could not be fully evaporated and the liquid droplets were trapped inside the wall of the main chamber (He, Davis and Illum, 1999). Moreover the polymer/extract ratio had also no significant effect on the responses. The limitation of this study was, the polymer/extract ratio could not be increased over 1.5/1. As the ratio was increased, the spray drying solution was too viscous and unable to feed into the drying chamber.

During the experiments, high percentage yields in the collector were observed when using an additive, colloidal silicon dioxide (Aerosil®), in the formulations. The formulations F9-19 (Table 5) which contained 0.25-0.50% Aerosil®, the percentage yields obtained from collector part were clearly higher than those from the cyclone part (Figure 20). This result might be explained that using Aerosil® in the formulations could modify the particles obtained from spray drying and thus improved flowability of microspheres from cyclone to collector part. Additionally for another reason, Aerosil® had anti-adherent property which could reduce the strong adhesion of the particles on the spray-dryer wall (Pohlmann et al., 2002). So, it only could improve the percentage yields in the collector part but with no significant effect.

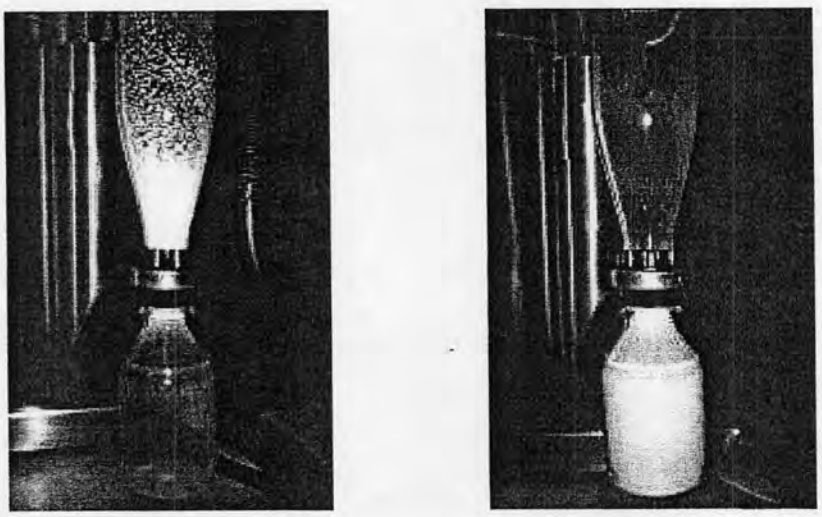

(a) **(b)**

Figure 20 Influence of additive (Aerosil®) on percentage yields in collector;
(a) no added Aerosil® in formulation
(b) added Aerosil® in formulation

2. Optimization design: central composite design (CCD)

In the second step, the two factors (inlet temperature and %solid content), were chosen to optimize %yield and %moisture content. While another parameters, feed rate, %additive and polymer/extract ratio, had less influence on the responses. So, they were fixed at the certain value in the further study. In this step, the non-significant parameters were fixed at flow rate 5 ml/min, polymer/extract ratio 1:1 and additive 0.5%, respectively.

To explore the region of the response surface in the neighborhood of the optimum, so that a second order approximation to the response surface could be developed. A central composite design was used for this purpose. The experiments of central composite design in this study was $2^2 + (2\times2) + 5 = 13$ runs. The design matrix with responses is given in Table 9.

Table 9 Central composite design matrix of two parameters and the observed responses

Code	Parameters		Responses	
	Inlet temperature (°C)	Solid content (%)	Total yield (%)	Moisture content (%)
C1	(-) 140	(-) 2	25.20	10.99 ±0.36
C2	(+) 160	(-) 2	31.36	8.89 ±0.06
C3	(-) 140	(+) 4	25.39	9.89 ±0.21
C4	(+) 160	(+) 4	37.21	7.83 ±0.09
C5	(-α) 136	(0) 3	28.62	11.31 ±0.10
C6	(α) 164	(0) 3	32.52	7.62 ±0.18
C7	(0) 150	(-α) 1.6	25.53	7.93 ±0.48
C8	(0) 150	(α) 4.4	28.43	8.17 ±0.34
C9	(0) 150	(0) 3	32.44	8.32 ±0.19
C10	(0) 150	(0) 3	38.29	8.61 ±0.13
C11	(0) 150	(0) 3	34.30	9.09 ±0.31
C12	(0) 150	(0) 3	33.86	7.90 ±0.12
C13	(0) 150	(0) 3	33.26	8.81 ±0.54

The second step, the percentage yields varied from 25.20-38.29%. In parallel, the moisture contents varied from 7.62-11.31%. The results of the second order, response surface quadratic model fitting in the form of analysis of variance for %yield and the linear model for %moisture content are given in Table 10 and Table 11, respectively. ANOVA was required to test the significance and adequacy of the model.

In the second step, the analysis of variance of the regression model demonstrate that the model of %yield and %moisture content were significant ($P < 0.05$). The response surface quadratic model was an adequate model for %yield and the linear model for %moisture content, as were evident from the F-test ($F_{\%yield} = 6.07$ and $F_{\%moist} = 10.45$) and a low probability values (%yield: $P_{model} > F = 0.018$ and %moisture content: $P_{model} > F = 0.004$) (Table 10 and Table 11). Values of "Prob > F" were less than 0.05 indicated that model terms were significant ($P < 0.05$) (Montgomery, 2001). Lack of fit for both models was not significant ($P > 0.05$). Non significant lack of fit was good (Stat-Ease Inc., 2005).

The goodness of fit of the models was checked by R^2. In this step, the values of $R^2 = 0.8125$ and 0.6763, indicated that 81.25% and 67.63% of variability in the response could be explained by the model for %yield and %moisture content, respectively.

The P-values were used as a tool to check the significance of each of the coefficients which were necessary to understand the pattern of the mutual interactions between the test variables (Montgomery, 2001). This implies that, result of %yield, the first order main effects of inlet temperature (A) and second order main effect of %solid content (B^2) were highly significant as were evident from their P-values = 0.012 and 0.008, respectively, so they were the most significant effects ($P < 0.05$) (Table 10). For moisture content, the first order main effect of inlet temperature was a significant effect as was evident from its P-value = 0.001 ($P < 0.05$) (Table 11).

Table 10 ANOVA for response surface quadratic model of % yield

Source of variations	Sum of squares	df	Mean square	*F*-value	Probability *P* (> *F*)
Model	184.285	5	36.857	6.068	0.018*
A-Inlet temp	69.004	1	69.004	11.360	0.012*
B-%solid content	12.856	1	12.856	2.116	0.189
AB	8.009	1	8.009	1.318	0.289
A^2	19.547	1	19.547	3.218	0.116
B^2	83.823	1	83.823	13.799	0.008*
Residual	42.521	7	6.074		
Lack of Fit	21.951	3	7.317	1.423	0.360**
Pure Error	20.570	4	5.143		
Corrected Total	226.807	12			

* Significant at *P value* = 0.05
** Not significant at *P value* = 0.05
*** R-Squared = 0.8125

Table 11 ANOVA for linear model of %moisture content

Source of variations	Sum of squares	df	Mean square	*F*-value	Probability *P* (> *F*)
Model	11.409	2	5.704	10.446	0.004*
A-Inlet temp	10.994	1	10.994	20.134	0.001*
B-%solid content	0.414	1	0.414	0.759	0.404
Residual	5.461	10	0.546		
Lack of Fit	4.622	6	0.770	3.677	0.114**
Pure Error	0.838	4	0.210		
Corrected Total	16.869	12			

* Significant at *P value* = 0.05
** Not significant at *P value* = 0.05
*** R-Squared = 0.6763

By applying multiple regression analysis on the experiment data, the experiment results of the central composite design were fitted with a second-order polynomial equation and linear equation for %yield and %moisture content, respectively. The coefficients of regression equation linking the responses to the experimental variables and interactions are indicated in Table 12.

Table 12 Coefficients of the regression equation linking the responses to the experimental factors and major interactions (coded units)

Responses	Parameters	Coefficients
%Yield	Intercept	34.43
	A-Inlet temp	2.94
	B-%solid content	1.27
	AB	1.42
	A^2	-1.68
	B^2	-3.47
%Moisture content	Intercept	8.87
	A-Inlet temp	-1.17
	B-%solid content	-0.23

Thus the mathmatical regression model for % yield and %moisture content fitted in the coded factors were given as following:

$$\%\text{Yield} = 34.43 + (2.94\times A) + (1.27\times B) + (1.42\times AB) - (1.68\times A^2) - (3.47\times B^2) \quad \text{.....(1)}$$

$$\%\text{Moisture content} = 8.87 - (1.17\times A) - (0.23\times B) \quad \text{.....(2)}$$

A and B were the coded values of the test variables;

A: inlet temperature

B: %solid content

From final equation in terms of coded parameters, this suggested that increasing inlet temperature improved the production of yield and using %solid content at range between 0 and 1 (the coded values) could improve the production of yield. Furthermore, it may be shown in the equation (1) that increasing of inlet temperature (A) improved the %yield while the term A^2 has no significance effect on %yield (Table10). The percentage yield of different value of the variables could be predicted from the response surface plot (quadratic model).

For %moisture content, the first order main effect of inlet temperature was a significant effect. This suggested that increasing inlet temperature was directly reduced residual moisture in the products. The moisture content could be predicted from linear regression plot (linear model). Figure 21 is the response surface plot for %yield and linear regression plot for %moisture content, respectively.

The normal probprability plot of the resdiuals is an important diagnostic tool to detect and explain the systematic departures from the assumptions that errors are normally distributed and are independent of each other and that the error variances are homogeneous (Montgomery, 2001). Figure 22 are normal probability plots of experiment results. The normal probability plot of the "Studentised" residuals indicated that some few violation of the assumptions outlying the analyses.

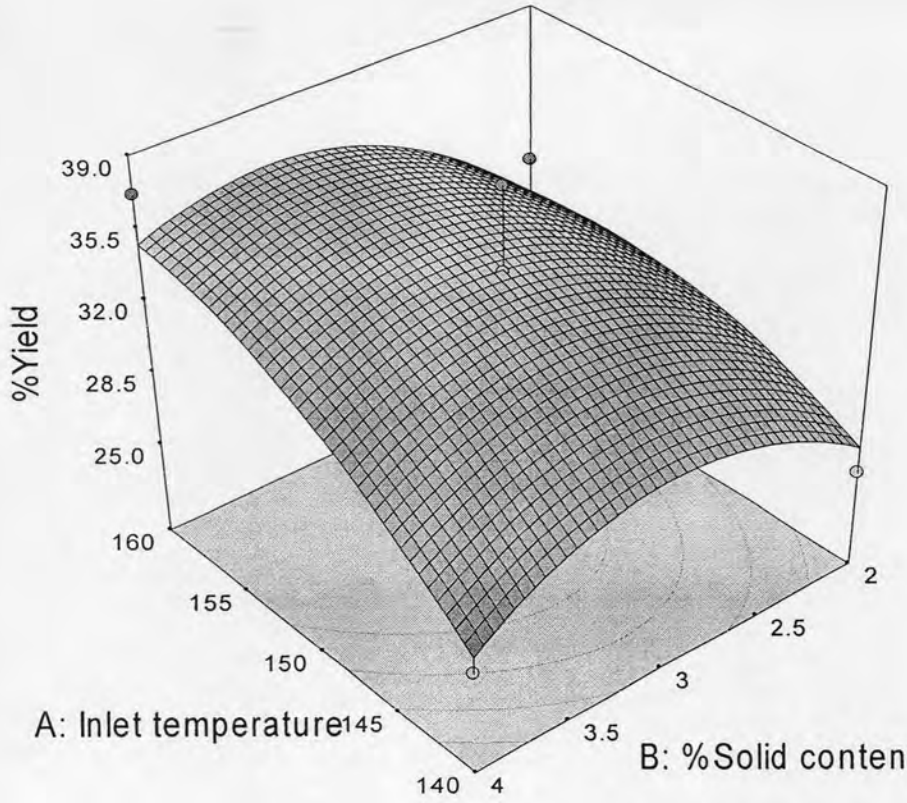

(a)

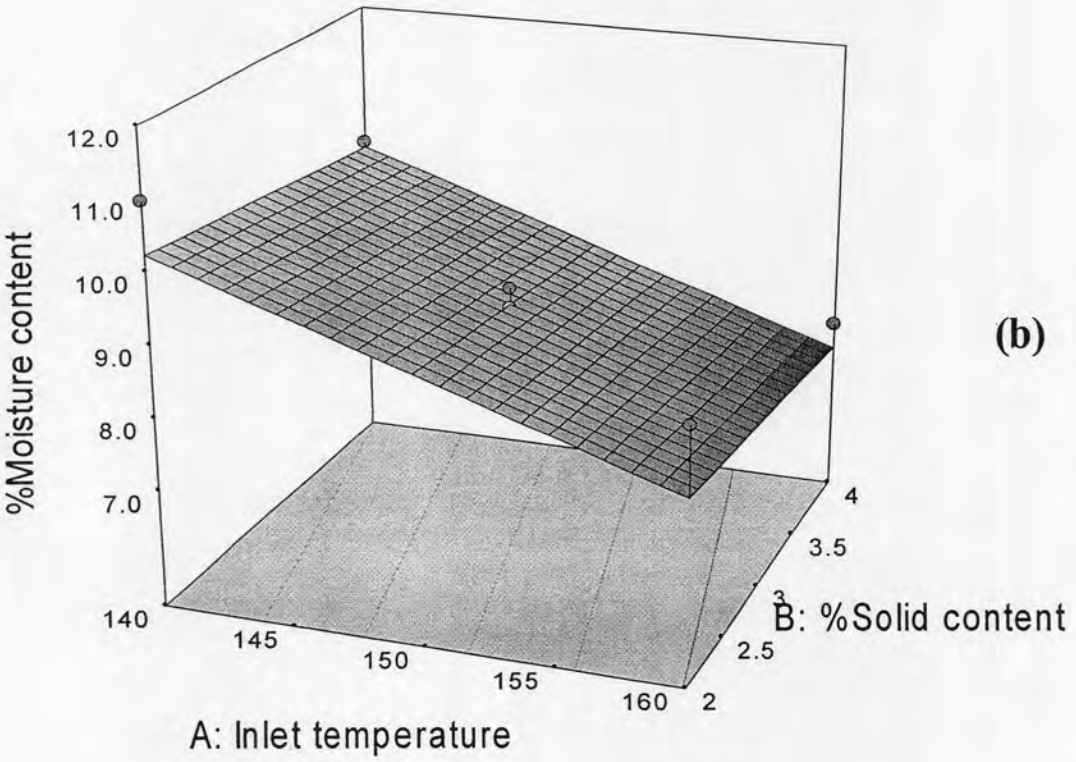

(b)

Figure 21 Response surface plot of % yield and linear regression plot of %moisture content; (a) response surface plot of % yield, (b) linear regression plot of %moisture content

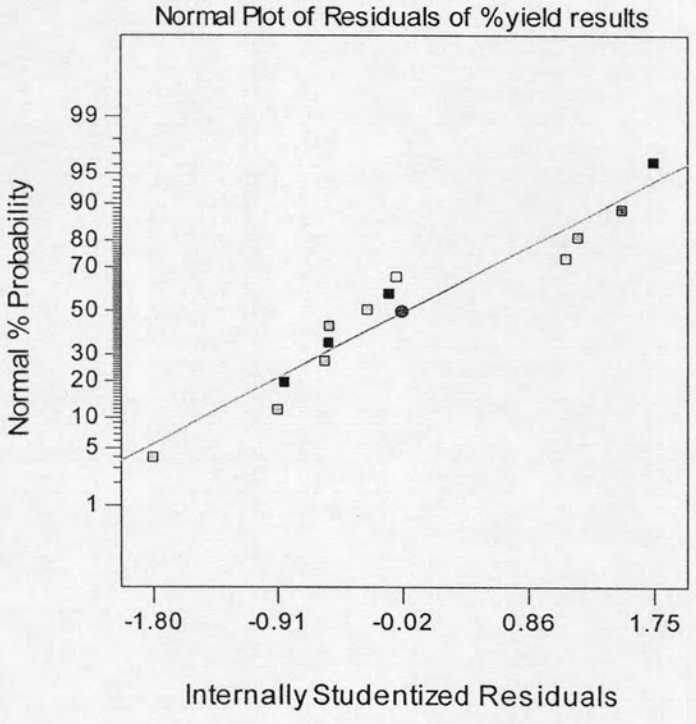

(a)

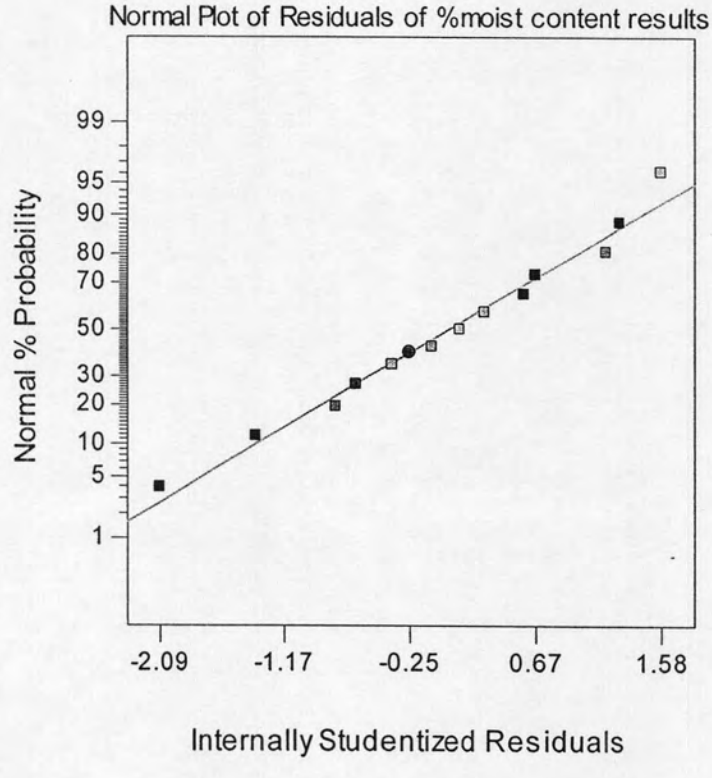

(b)

Figure 22 The normal probability plots of the %yield and %moisture content;

(a) The normal probability plot of the %yield results

(b) The normal probability plot of the %moisture content results

Based on the two models obtained, a graphical optimization was also conducted using the Design-Expert version 7.0.3 statistical software. Recall, the main objective was to obtained %yield as high as possible and %moisture content as low as possible. The selection of conditions to overlay plot were range from 140-160 °C and 2-4 % for inlet temperature and solid content, respectively. The method basically consisted of overlaying the curves of the models accroding to the criteria imposed. The criterias were adopted:

(a) %yield higher than 38.29% (the highest %yield in a second step)

(b) %moisture content lower than 7.62% (the lowest %moisture content in a second step)

As considering the inverse relationship between %yield and %moisture content. The attained overlaying plot showed a non-shaded area (white area) where both criterias imposed were satisfied (Figure 23). Thus, a point was chosen on the graph (marked by the square). This point was assigned as optimum point and corresponded to 160°C inlet temperature and 3.4 %solid content. Under these conditions, the model predicted 36.21 %yield (a variation of = 32.98 - 39.43% being possible) and 7.62 %moisture content (a variation of = 6.83 – 8.39% being possible) in the confidence range of 95%.

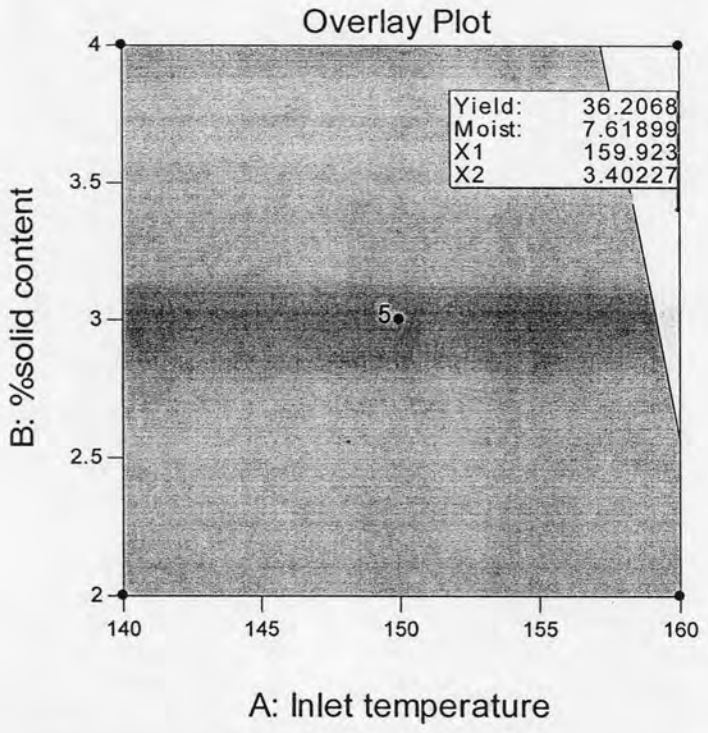

Figure 23 The optimum region by overlay plot of two responses (%yield and %moisture content) evaluated as a function of inlet temperature and %solid content

The statistical interpretation of the results concerning both yield and moisture content using the response surface methodology led us to the choice of optimal operating condition. These parameters had to maximize yields while reducing moisture contents.

To confirm the result, three batches were produced using the optimal conditions to validate the fabrication process (Table 13).

Table 13 The optimum region by overlay plot of two parameters and the observed responses

Code	Parameters		Responses	
	Inlet temperature (°C)	Solid content (%)	Total yield (%)	Moisture content (%)
O1	160	3.4	36.30	7.89
O2	160	3.4	34.99	8.58
O3	160	3.4	35.55	8.27

The results in Table14 are showed, the observed means and standard deviations of the responsed obtained for yield and moisture content were found to be 35.61±0.66% and 8.25±0.35%, respectively. They were in range of the prediction intervals at 95% confidence level. These results clearly showed that the model fitted the experimental data well and described the region studied well.

Table 14 Observed responses and 95% CI (confidence interval) of optimization formulation

Responses	Values		
	%Observed	%Predicted	95% confidence intervals
Total yield (%)	35.61 ±0.66	36.21	32.98 – 39.43
Moisture content (%)	8.25 ±0.35	7.62	6.83 – 8.39

The optimal microspheres obtained as fine particles with pale-yellow color and powder bulkiness were demonstrated in Figure 24.

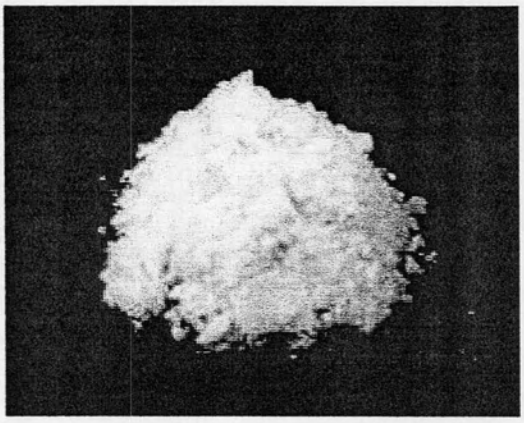

Figure 24 Powders of optimal formulation from optimization design

B. Evaluation of Physicochemical Properties of Spray Dried Microspheres

1. Morphology of spray dried microspheres

The shape and surface topography of the spray dried particles were found to be affected by the formulation and processing parameters. The observation of size, shape and surface topography were done by scanning electron microscopy (SEM). Figure 25 showed the scanning electron photomicrographs of raw material of chitosan, centella extract and Aerosil® at different magnifications. The chitosan was in irregular flakes of different sizes with smooth surface. Centella extract was in irregular shapes of various sizes. Aerosil® was in very fine particles and loosely agglomerate together.

The shape and surface topography of chitosan microspheres and pure centella extract microspheres are displayed in Figure 26. The scanning electron photomicrograph showed both spray-dried particles were obtained as very small spheres. The surface of pure centella extract microspheres was smooth but of chitosan microspheres was slightly shrunk. Figure 27-32 showed the scanning electron photomicrographs of microspheres prepared by fractional factorial design (F1-F19) and the optimal formulation.

The sphericity of particles obtained from the formulation F1-F8 was good. The surface of the microspheres was smooth and the crystal of centella extract on the surface was not observed. However the shape irregularity of microspheres was met in some formulations (F9-F16 and optimal formulation) that added additive. The results could be explained that the formulations of pure centella extract microspheres and centella-chitosan microspheres were prepared by dissolved in co-solvent solution (5% propylene glycol, 10% absolute ethanol and distilled water) which the propylene glycol behaved as a plasticizer could reduce the surface tension of spray drying solution. Solution with lower surface tension required less energy to form the separated spherical droplets from the nozzle of spray dryer that could give the spherical microspheres (Swarbrick and Boylan, 1996). Moreover in process of spray drying, plasticizer in formulation retained some water molecules linked to its own structure and could fill the intern empty space of the microspheres, preserving the hydration, slow evaporation of solvent within the droplets avoiding depression on the surface, and assuring a more uniform wall and spherical shape of the obtained microspheres (Bruschi et al., 2003). As a parallel, the shrinkage of the surface wall was the result of water loss from the drying droplets

during the early stage of processing. This result was consistent with a previous study by Columbano, Buckton and Wikeley (2003).

However, in formulation adding Aerosil®, agglomerate particles of Aerosil® were observed. Similar results from solid dispersion of tolbutamide prepared with fine silica particles by spray drying were reports (Takeuchi et al., 2004). The result could be explained that Aerosil® was a fine, light and amorphous powder consisting of primary particles in the nanometer range (10-40 nm), resulting in a very large specific surface area (from 50-400 m^2/g). The primary particles were not isolated but fused together in relatively stable chain-like aggregates, which in turn form larger agglomerates (Jonat, 2005).

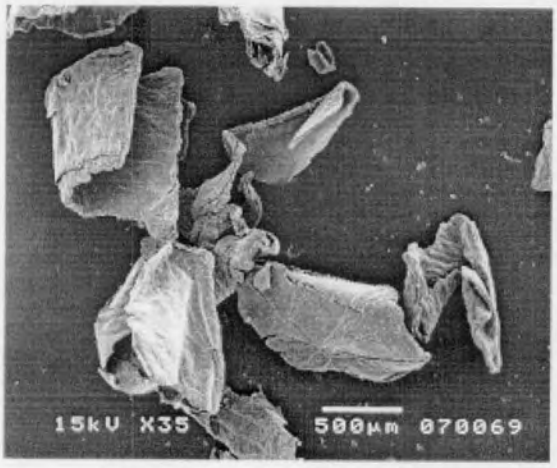

(a) (×35)

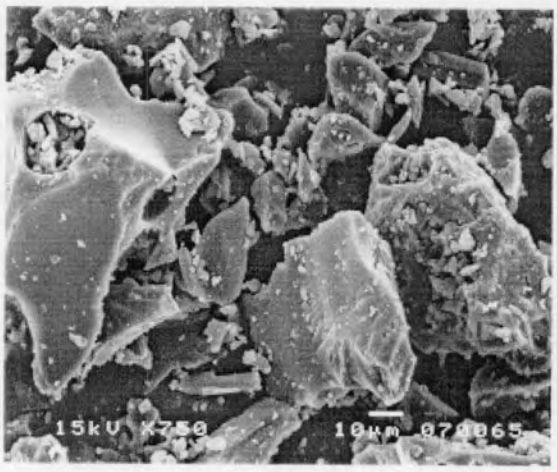

(b) (×750)

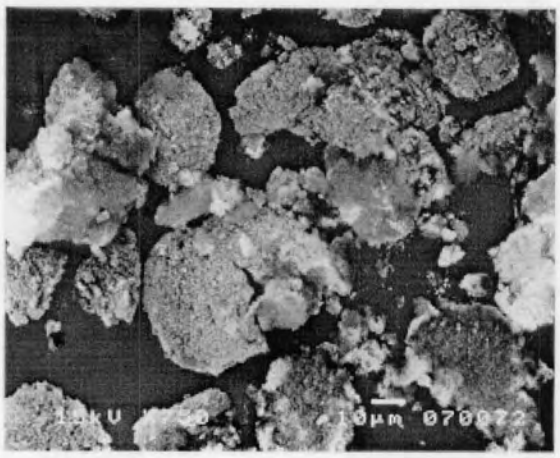

(c) (×750)

Figure 25 Scanning electron photomicrographs of raw materials;
(a) chitosan flakes, (b) centella extract, (c) Aerosil®

(×2000)

(a)

(×2000)

(b)

Figure 26 Scanning electron photomicrographs of microspheres prepared without additive in formulation;

(a) chitosan microspheres prepared from 1%chitosan solution

(b) centella microspheres prepared from 1% centella extract solution

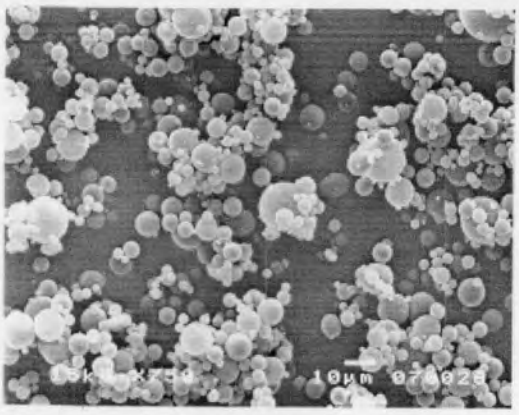

(×750)

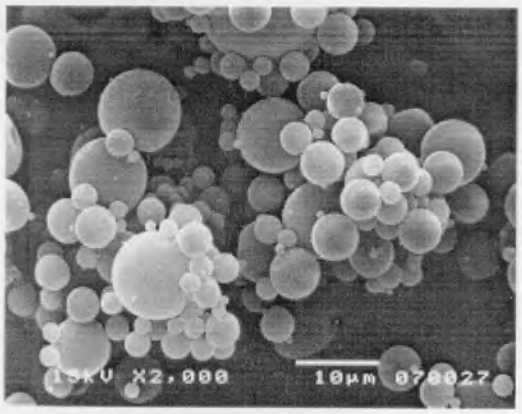

(×2000)

(a) F1

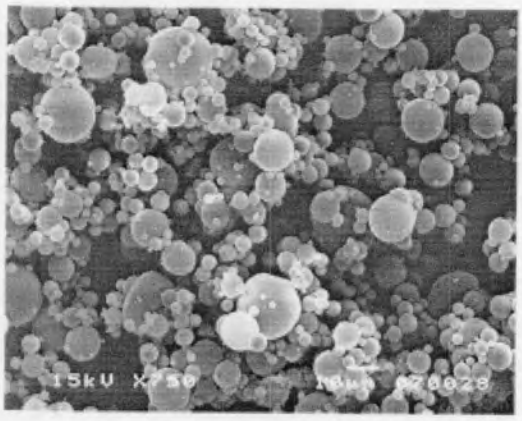

(×750)

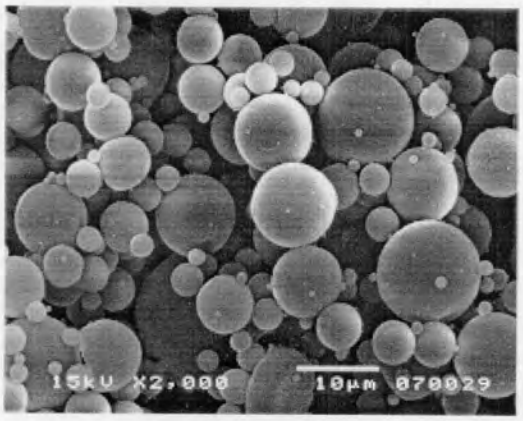

(×2000)

(b) F2

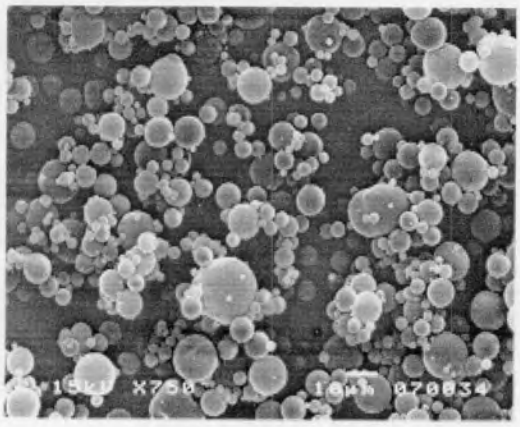

(×750)

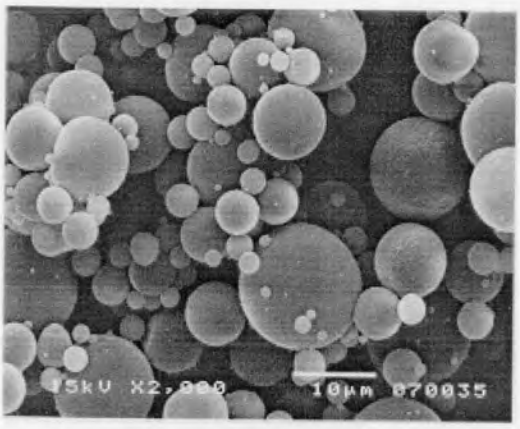

(×2000)

(c) F3

Figure 27 Scanning electron photomicrographs of microspheres prepared from experimental design; (a) F1, (b) F2, (c) F3

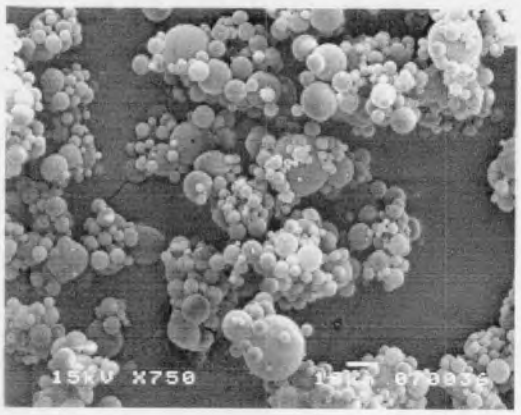

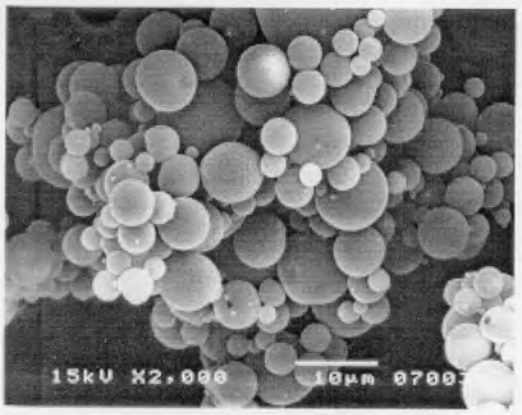

(×750) (×2000)

(a) F4

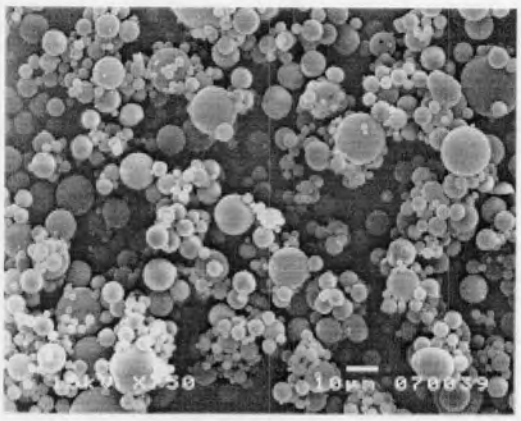

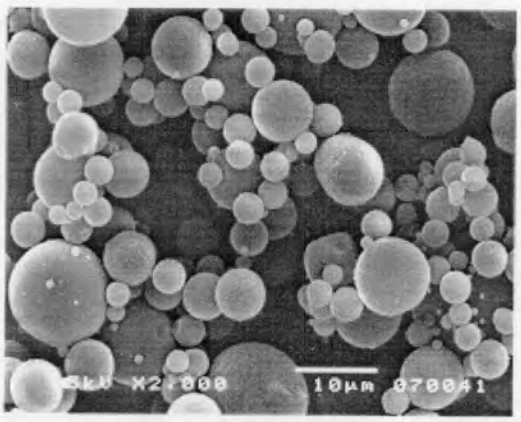

(×750) (×2000)

(b) F5

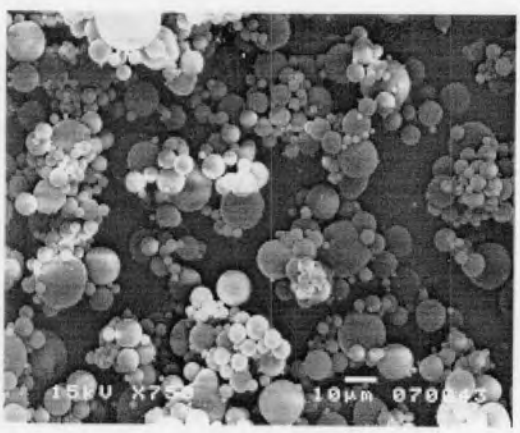

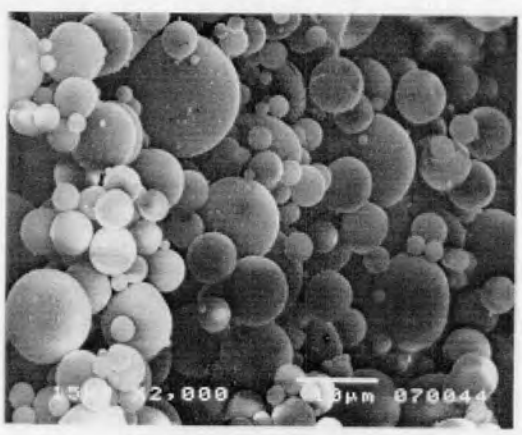

(×750) (×2000)

(c) F6

Figure 28 Scanning electron photomicrographs of microspheres prepared from experimental design; (a) F4, (b) F5, (c) F6

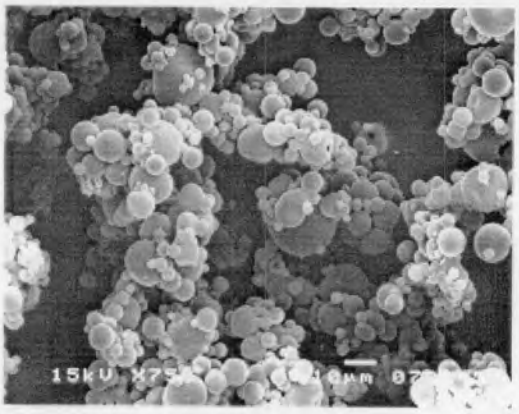

(×750)

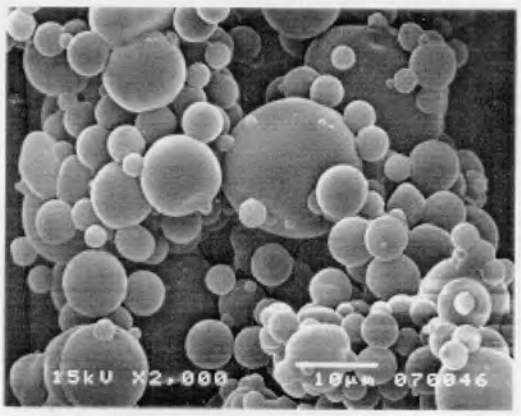

(×2000)

(a) F7

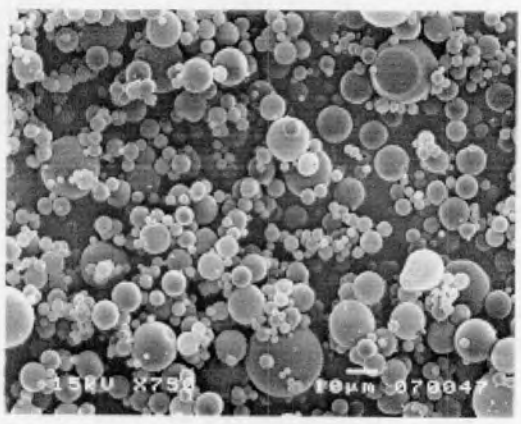

(×750)

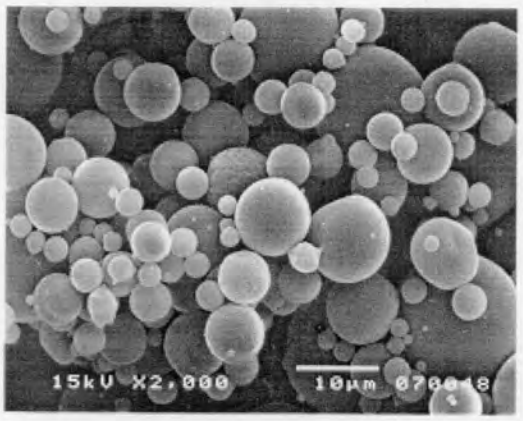

(×2000)

(b) F8

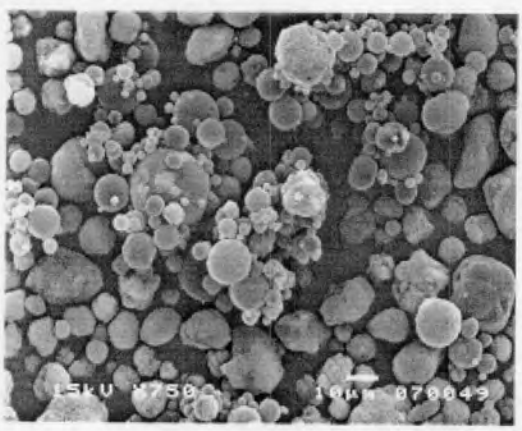

(×750)

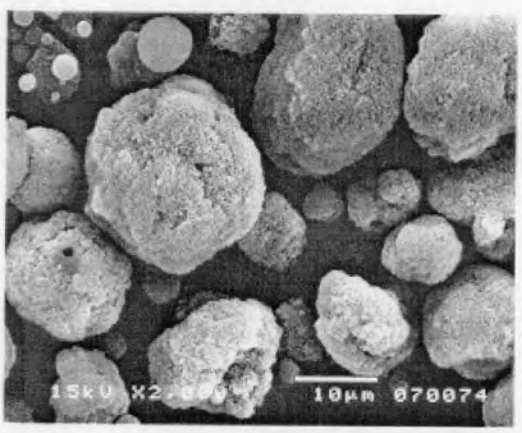

(×2000)

(c) F9

Figure 29 Scanning electron photomicrographs of microspheres prepared from experimental design; (a) F7, (b) F8, (c) F9

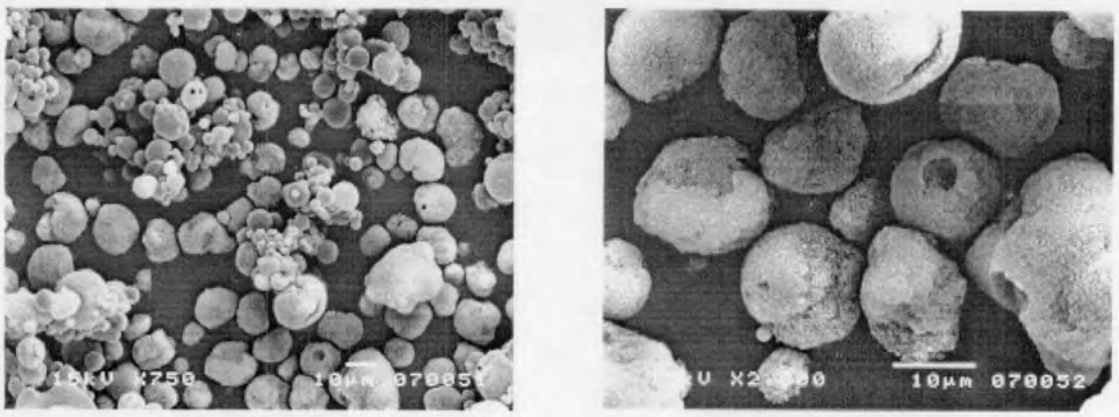

(×750) (×2000)

(a) F10

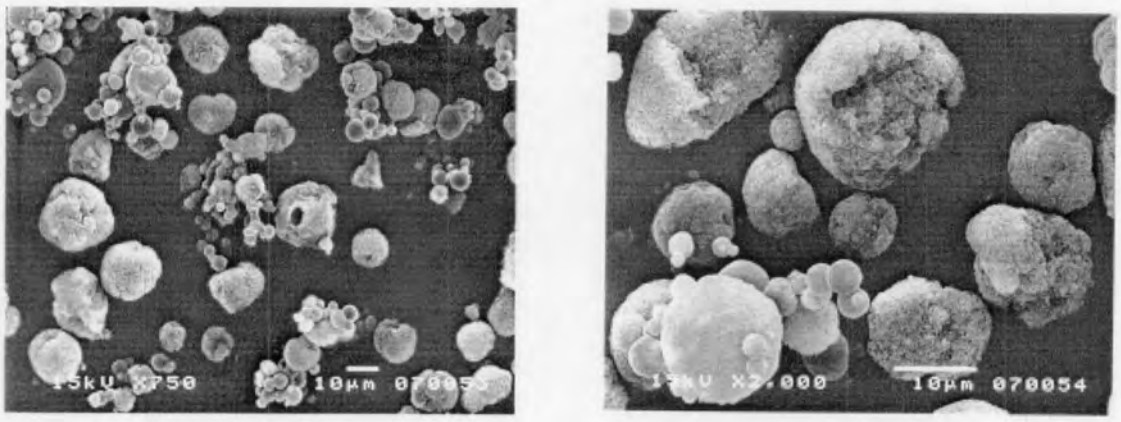

(×750) (×2000)

(b) F11

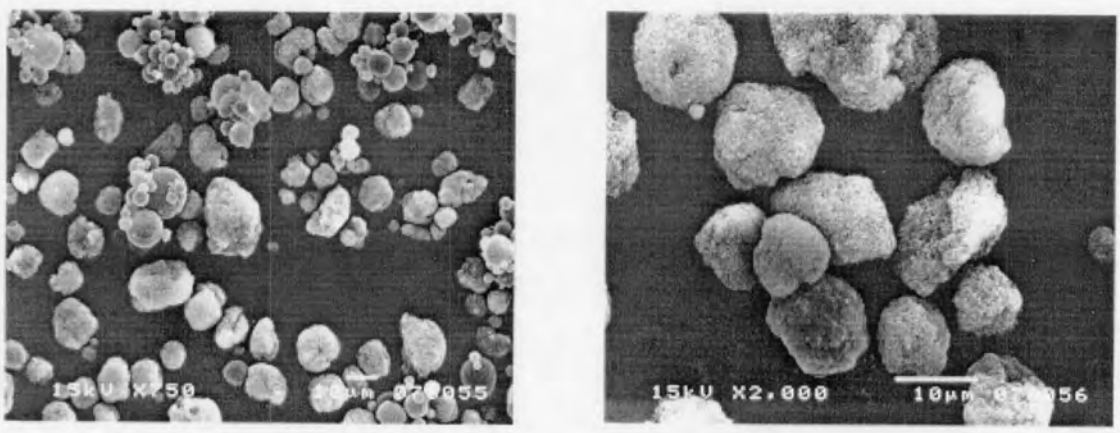

(×750) (×2000)

(c) F12

Figure 30 Scanning electron photomicrographs of microspheres prepared from experimental design; (a) F10, (b) F11, (c) F12

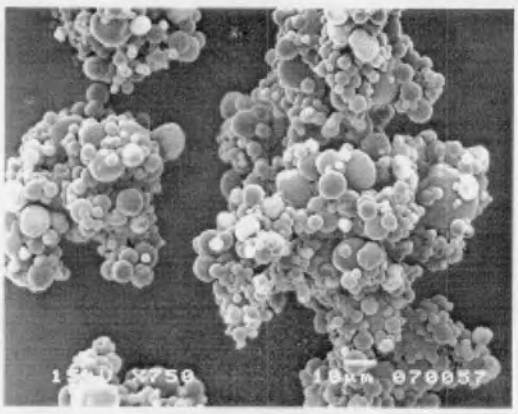

(×750)

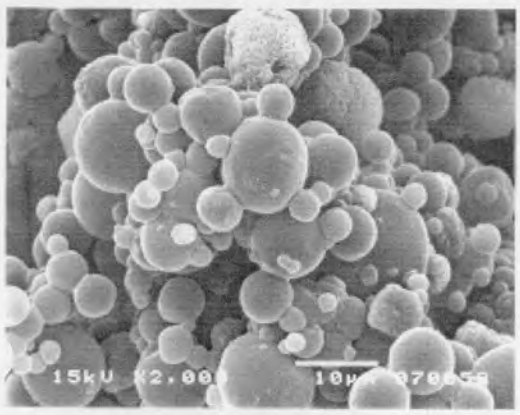

(×2000)

(a) F13

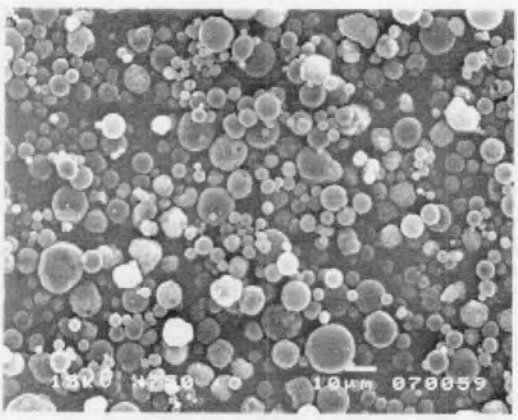

(×750)

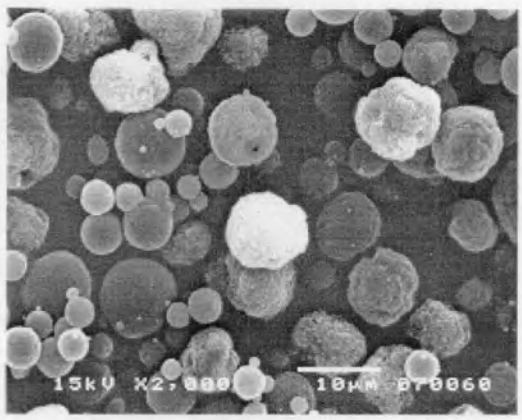

(×2000)

(b) F14

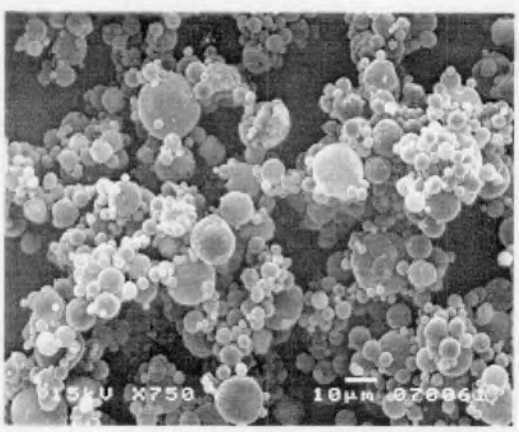

(×750)

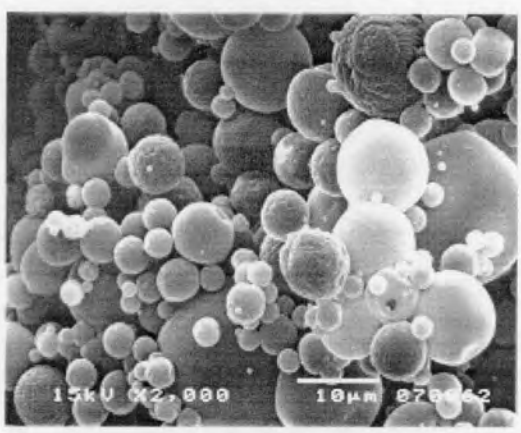

(×2000)

(c) F15

Figure 31 Scanning electron photomicrographs of microspheres prepared from experimental design; (a) F13, (b) F14, (c) F15

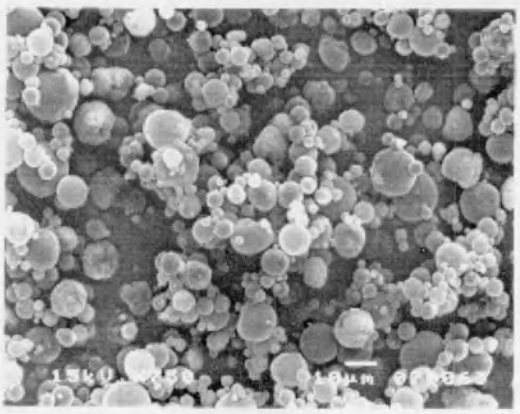

(×750)

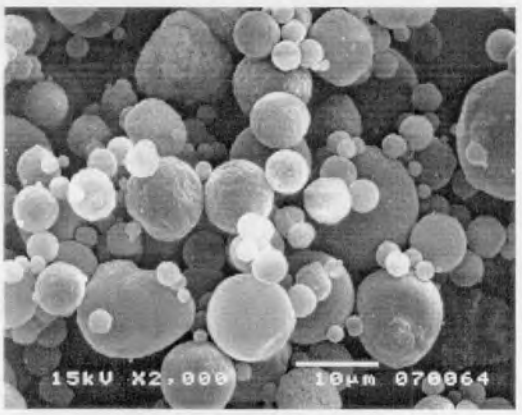

(×2000)

(a) F16

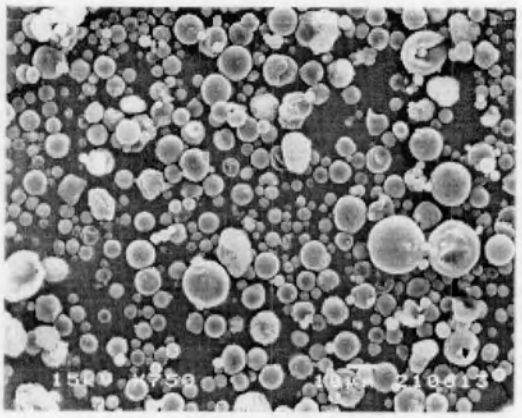

(×750)

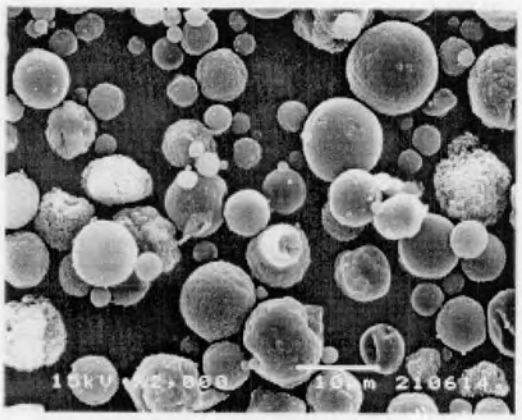

(×2000)

(b) optimal formulation

Figure 32 Scanning electron photomicrographs of microspheres prepared from experimental design; (a) F16, (b) optimal microspheres

2. Particle size and size distribution

Usually, spray-dried powders were obtained in a median diameter range between 2 and 50 micron with a narrow size distribution (Broadhead, Rouan and Rhodes 1992). In this study, the average particle size (D [4, 3]) and particle size distribution (Span value) were determined and compared between different formulations of spray-dried microspheres. The particle sizes were range from 9.47±0.04 to 166.10±2.08 μm and the span values ranged from 1.34±0.02 to 7.84±0.21 μm (Table 15).

Table 15 The particle size distributions of the spray-dried microspheres (n=3)

Formulation code	Average particle size	
	D [4, 3] ± SD (μm)	Span ± SD (μm)
F1	10.53 ± 0.29	1.50 ± 0.01
F2	11.22 ± 0.04	1.61 ± 0.01
F3	41.88 ± 0.18	2.85 ± 0.04
F4	14.04 ± 0.09	1.34 ± 0.01
F5	15.56 ± 0.14	7.21 ± 0.04
F6	16.29 ± 0.17	7.56 ± 0.37
F7	126.58 ± 1.29	2.10 ± 0.02
F8	22.88 ± 0.19	1.57 ± 0.02
F9	16.45 ± 0.05	2.26 ± 0.01
F10	65.10 ± 2.76	2.89 ± 0.11
F11	76.41 ± 1.10	3.17 ± 0.07
F12	39.70 ± 0.18	3.60 ± 0.01
F13	166.10 ± 2.08	2.41 ± 0.05
F14	9.47 ± 0.04	1.37 ± 0.01
F15	49.37 ± 0.05	3.65 ± 0.05
F16	21.01 ± 0.44	7.84 ± 0.21
Optimal microspheres	5.19 ± 0.02	1.42 ± 0.02

By the SEM observation, it showed the size of the microspheres ranged from 5–10 μm at all formulations. However it was noticed that the particle size obtained from the light scattering method was larger than those observed from the SEM method. Since the aggregation of microspheres was clearly observed in the formulations with high moisture contents, thus a larger mean of diameter was detected from the light scattering method compared to the actual particle size. However it was noticed that the particle size of optimal formulation obtained from the light scattering method and the SEM method were similar results (Figure 32b and Table 15). It implied that the aggregation did not occur.

Consequently, spray-dried microspheres with higher moisture content resulted larger particle sizes as measured by the light scattering method. This is demonstrated by a scattered plot between particle size and percentage moisture content depicted in Figure 33.

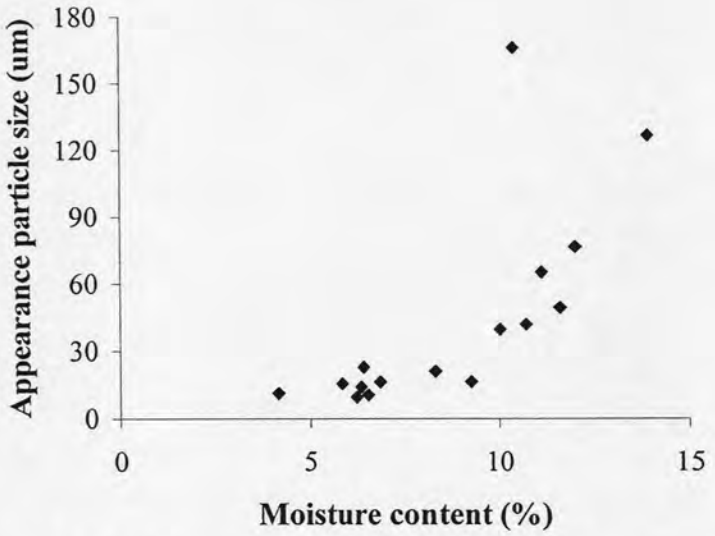

Figure 33 A scattered plot between %moisture content and appearance particle size of spray-dried microspheres

The aggregation occurred when the droplets could not separate from each other during drying process. The result might be explained that feed rate used was too high that led to ineffective atomization. Furthermore, increasing concentration of spray solution and adding an additive in spray-dried microspheres resulted in large particle sizes. This might be attributed to the effect of appeared viscosity of spray solution. If the viscosity of spray solution was too high, an extrusion process occured, resulting in "spaghetti" structures (such as Figure 31a). This might cause and resulted in

aggregation (Lacasse, Hildgen and McMullen, 1998). Scattered plot between viscosity of spray solution and appeared particle size of spray-dried microspheres is depicted in Figure 34.

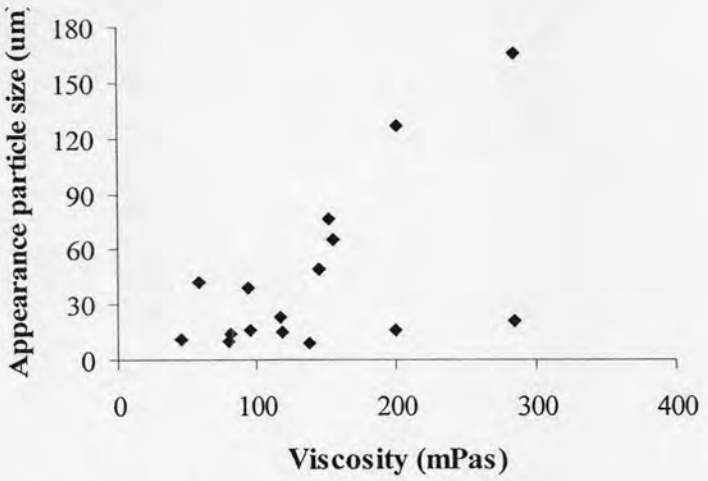

Figure 34 A scattered plot between viscosity of spray solution and appearance particle size of spray-dried microspheres

3. Zeta potential

The zeta potential of microspheres was measured in phosphate buffer solution pH 7.4 (0.0001 M). The results obtained are presented in Table 16. Also as the control, the zeta potential of ethylcellulose microspheres was measured in the same medium which was -72.68±1.03 mV. The negative zeta potential of ethyl cellulose microspheres in some medias such as acetate buffer (pH 4) and phosphate buffer (pH 7) was previously reported (He, Davis and Illum, 1998). The additive Aerosil®, colloidal silicon dioxide, showed the negative zeta potential (-31.94±0.08 mV). Blank chitosan microspheres gave the highest positive zeta potential (42.34±0.98 mV) which was as expected since chitosan free amino groups were responsible for the measured positive zeta potential (Berthold, Cremer and Kreuter, 1996).

All chitosan microspheres with centella extracts obtained were positively charged, indicating the charge property of chitosan at the surface of all microspheres. The zeta potentials of sample microspheres were ranged between 20.94±0.58 and 35.51±0.78 mV. For some formulations containing Aerosil® (F9-F16 and optimal microspheres), the zeta potential was lower than the corresponding formulation without Aerosil®. It could be explained by partial presence or random deposit of Aerosil® at the surface of the microspheres. This was confirmed by scanning electron photographs

(Figure29c-Figure32). Similar result had been reported that spray dried chitosan-ethylcellulose microspheres had reduced zeta potential due to the partial presence of ethylcellulose at the surface of microspheres (Martinac et al., 2005).

It was important to conclude that the zeta potentials of all sample microspheres prepared were positive, indicating the presence of chitosan at the surface of the microspheres. The observation was of great importance, since positive charges from chitosan were necessary for the interaction with negatively charged mucus and consequently, mucoadhesion. Furthermore, factors leading to a reduction of zeta potential led to a reduction of mucoadhesive property (He, Davis and Illum, 1998).

Table 16 Zeta potentials of spray-dried centella microspheres and some compounds (n=3)

	Formulation code	**Zeta potential (mV)**
Without additive	F1	30.31 ± 0.71
	F2	33.51 ± 0.16
	F3	30.33 ± 1.48
	F4	28.73 ± 0.46
	F5	30.27 ± 0.45
	F6	30.04 ± 1.32
	F7	31.18 ± 0.91
	F8	32.32 ± 1.45
With additive	F9	29.89 ± 1.64
	F10	20.94 ± 0.58
	F11	26.42 ± 0.43
	F12	32.53 ± 0.98
	F13	27.00 ± 2.21
	F14	35.51 ± 0.78
	F15	25.52 ± 1.19
	F16	32.88 ± 0.86
	Optimal microspheres	32.87 ± 1.39
	Chitosan microspheres	42.34 ± 0.98
	Ethylcellulose microspheres	-72.68 ± 1.03
	Aerosil® powder	-31.94 ± 0.08

4. In vitro evaluation of mucoadhesive property of microspheres

The mucoadhesive property was studied in vitro using pig rectum. The photographs showing the adhesion on mucous membrane of centella microspheres (no polymer), ethylcellulose microspheres (as control), optimal microspheres and optimal microspheres dispersed in liquid suppository base are dispicted in Figure 35. It was found that the centella microspheres without polymer and ethylcellulose microspheres were rapidly washed out and disappeared from the pig rectum within 5 minutes. The obviously longer residence time of 240 minutes were observed from the optimal microspheres and optimal microspheres dispersed in liquid suppository (Table 17). This revealed the high mucoadhesive property of chitosan microspheres on mucus membrane. This result agreed with a previous study that spray-dried propranolol mucoadhesive microspheres, formulations containing chitosan, adhered more than 300 minutes on pig intestinal tissue (Harikarnpakdee, 2003). This suggested that mucoadhesive polymer was very important for adhering with mucus layer. So, chitosan was the most factors for mucoadhesive property in this investigation as regarding of adhesion time.

Table 17 The adhesion times of microspheres adhered on mucus surface of pig rectum

Formulation	Adhesion time (min)
Centella microspheres	5
Ethylcellulose microspheres	5
Optimal microspheres	>240
Optimal microspheres dispersed in liquid suppository	>240

Chitosan is comprised of one primary amino and two free hydroxyl groups for each C_6 building unit that can give rise to hydrogen bonding and the linear molecule expresses sufficient chain flexibility. The conformation was highly dependent on ionic strength. These properties are considered essential for mucoadhesion (Peppas and Buri, 1985; Robinson and Mlynek, 1995).

Furthermore, the cationic polyelectrolyte nature of chitosan could provide a strong electrostatic interaction. Electrostatic attraction was thought to play an important role, because the adhesion of mucin and chitosan was expected to be domain by the electrostatic interaction between the positively charged chitosan and negatively

charged mucin (He, Davis and Illum, 1999). These results conform to the positive zeta potential reported in the previous section. Moreover, He, Davis and Illum (1998) reported that an increase in the charge density of chitosan resulted in adhesive properties becoming more marked and the charge density of chitosan in a formulation was affected by its degree of deacetylation and any cross-linking treatment. Chitosan adhesive property should become more marked as increasing degree of deacetylation and avoidance cross-linking procedure. These findings confirmed good mucoadhesive property of optimal microspheres in this study, which 95% degree of deacetylation and avoidance cross-linking treatment of chitosan were selected. Basic studies on bioadhesive delivery systems for peptide drugs of Bernkop-Schnürch, Humenberger and Valenta (1998) had also indicated that cross-linking reduced mucoadhesive effects of chitosan.

In vitro evaluation of mucoadhesive property of microspheres

0 min 1 min 5 min

(a) centella microspheres

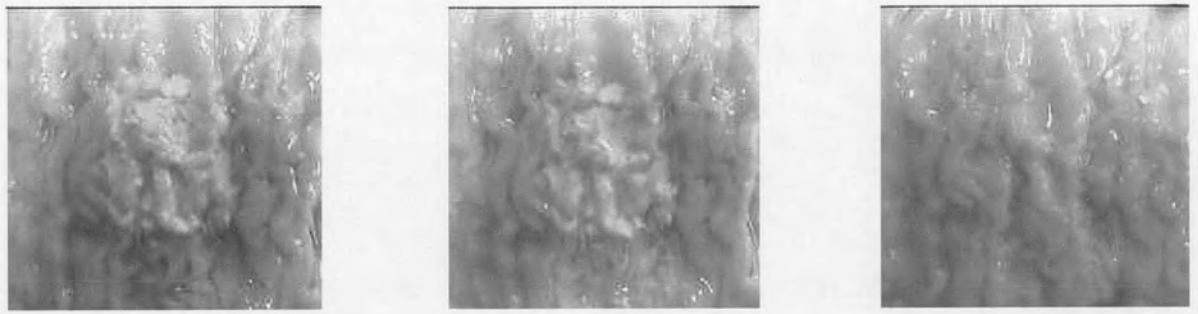

0 min 1 min 5 min

(b) ethylcellulose microspheres

Figure 35 The photographs of mucoadhesive microspheres adhered on mucus surface of pig rectum at difference time; (a) centella microspheres, (b) ethylcellulose microspheres

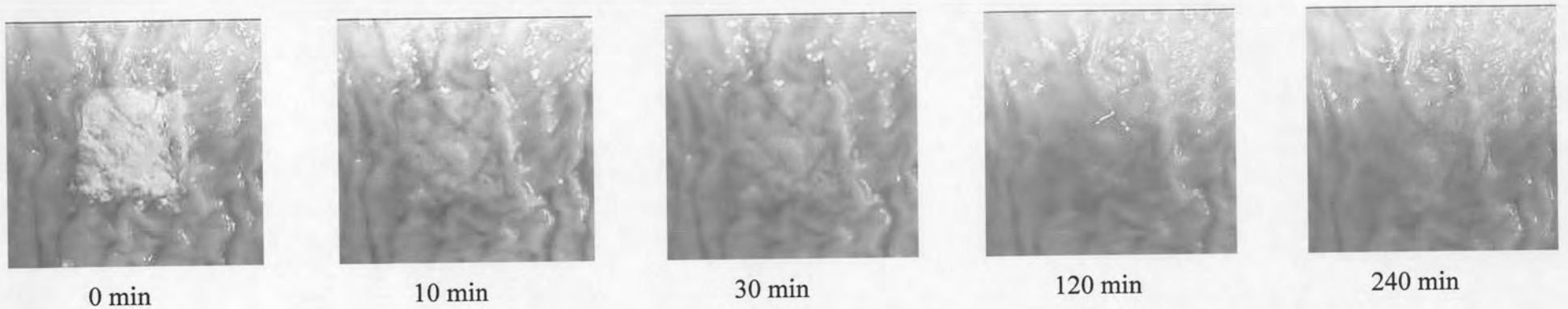

(c) optimal microspheres

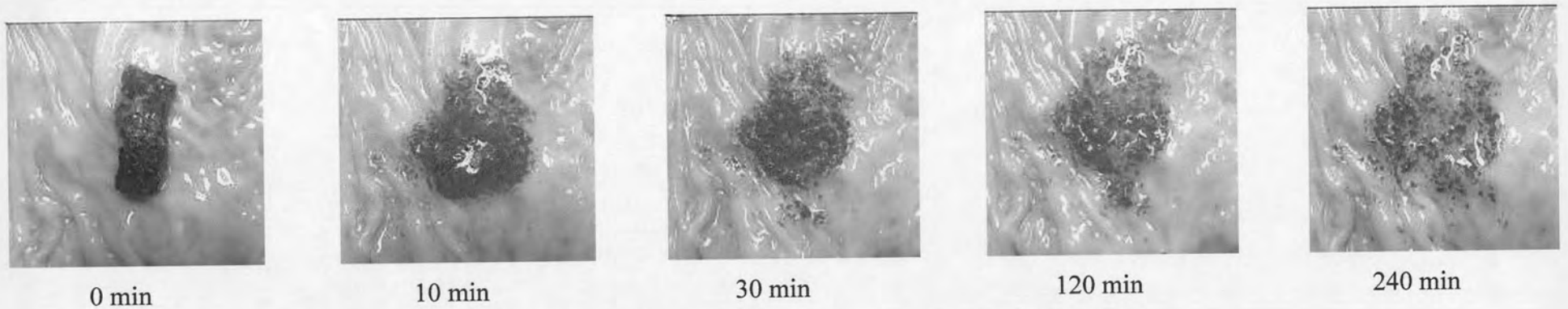

(d) optimal microspheres dispersed in liquid suppository

Figure 36 The photographs of mucoadhesive microspheres adhered on mucus surface of pig rectum at difference time (continued);
(c) optimal microspheres, (d) optimal microspheres dispersed in liquid suppository

5. Differential scanning calorimetry

The DSC thermograms of standard asiaticoside, standard madecassoside, centella extract, physical mixture of centella extract with chitosan ratio 1:1 and 1:1.5, blank chitosan microspheres, chitosan microspheres containing centella extract (F1-16) and optimal formulation microspheres are shown in Figures 37-39.

The thermograms of standard asiaticoside and standard madecassoside demonstrated endothermic peaks, which might be attribute to melting at 243.05°C and 230.68°C, respectively. This showed that the two compounds existed in crystalline form (Figure 37a and 37b). The DSC thermogram of the centella extract showed the endothermic melting peaks with broad range of temperature were 230.02°C and 238.19°C (Figure 37c). This result indicated the existence of madecassoside and asiaticoside in crystalline form in the extract. These endothermic peaks disappeared in the centella spray-dried microspheres (Figure 37f) which revealed that spray drying process promoted the existence of amorphous form of the extract. Chitosan microspheres exhibited no melting peak. The DSC thermogram of chitosan microspheres showed a halo pattern. This revealed that they were in amorphous state. Additionally the endothermic peak of centella extract disappeared in the physical mixtures. This might be due to possible interaction between centella extract and chitosan. This result agreed with a previous study regarding chitosan microspheres containing theophylline (Asada et al., 2004).

No endothermic peak corresponding to centella extract melting was observed in the thermograms of F1–F16 and optimal formulations (Figures 36-37). The results might be explained that the centella extract in chitosan spray dried matrix particles was uniformly dispersed in amorphous state. Similar result was reported from spray-dried microspheres of paclitaxel (Mu et al., 2005).

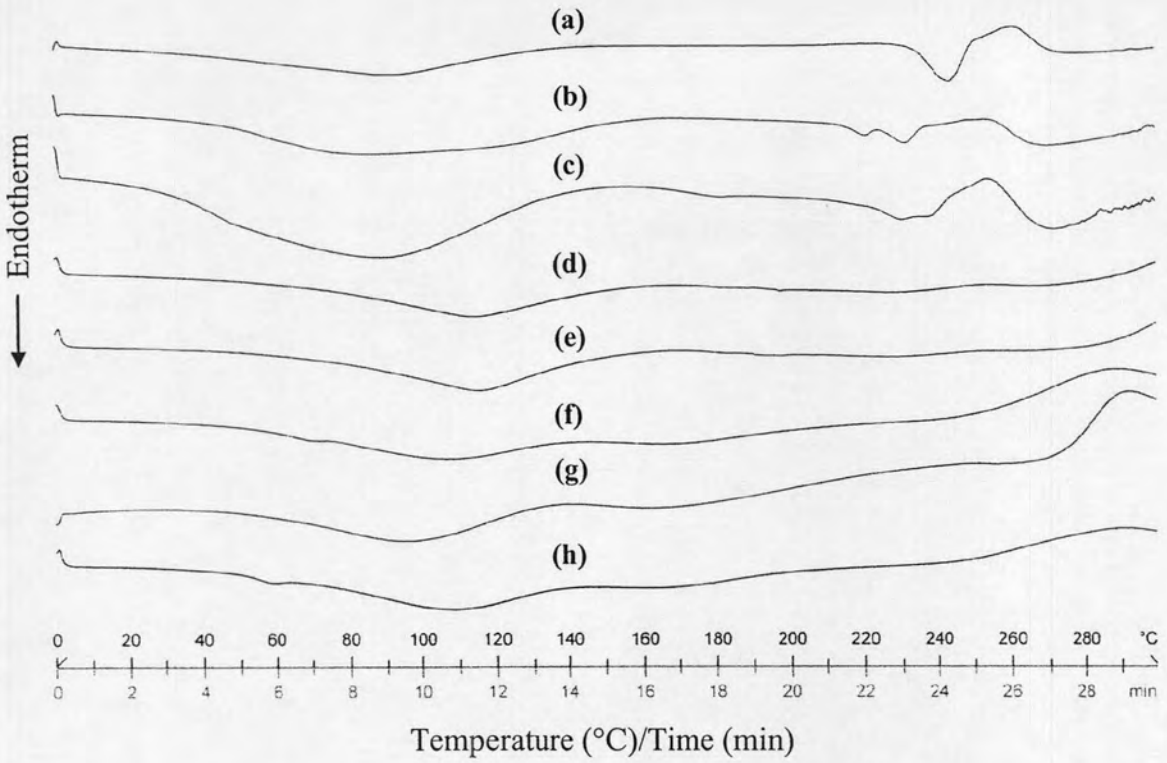

Figure 37 The DSC thermograms of standard asiaticoside, standard madecassoside, centella extract, physical mixture of centella extract with chitosan ratio1:1 and 1:1.5, centella microspheres, chitosan microspheres and optimal formulation;

(a) standard asiaticoside

(b) standard madecassoside

(c) centella extract

(d) chitosan:centella extract ratio 1:1 by weight

(e) chitosan:centella extract ratio ratio 1.5:1 by weight

(f) centella spray-dried microspheres

(g) chitosan spray-dried microspheres

(h) optimal formulation microspheres

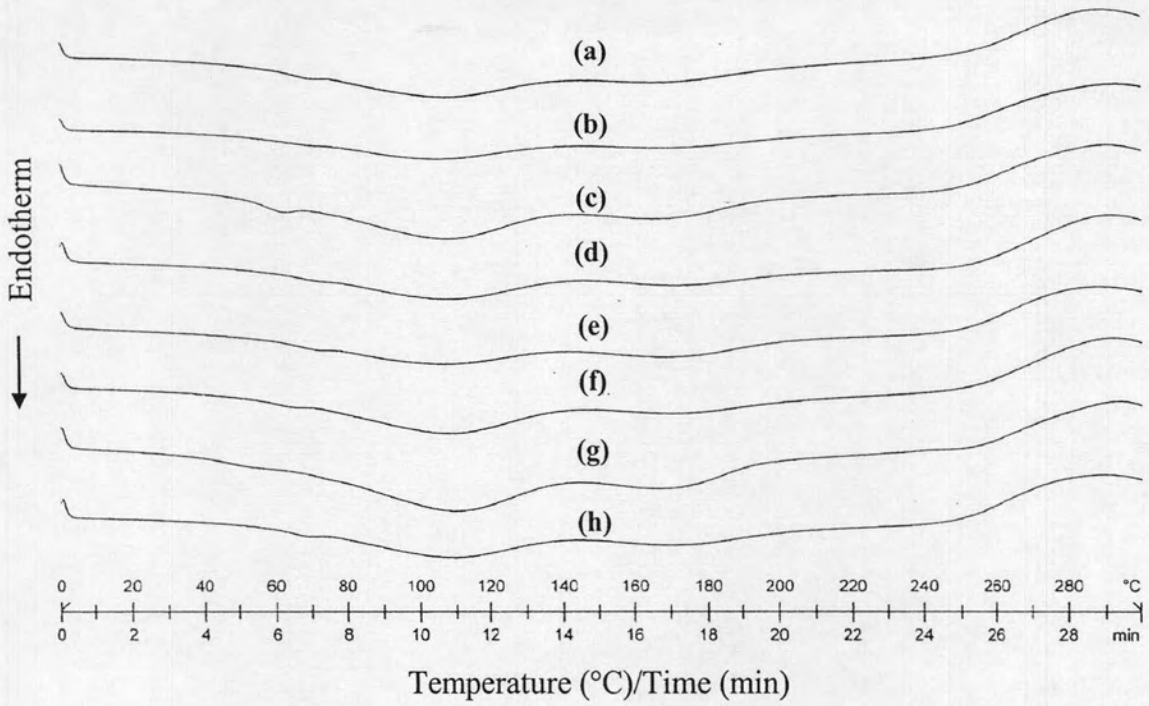

Figure 38 The DSC thermograms of F1-F8;

(a) F1

(b) F2

(c) F3

(d) F4

(e) F5

(f) F6

(g) F7

(h) F8

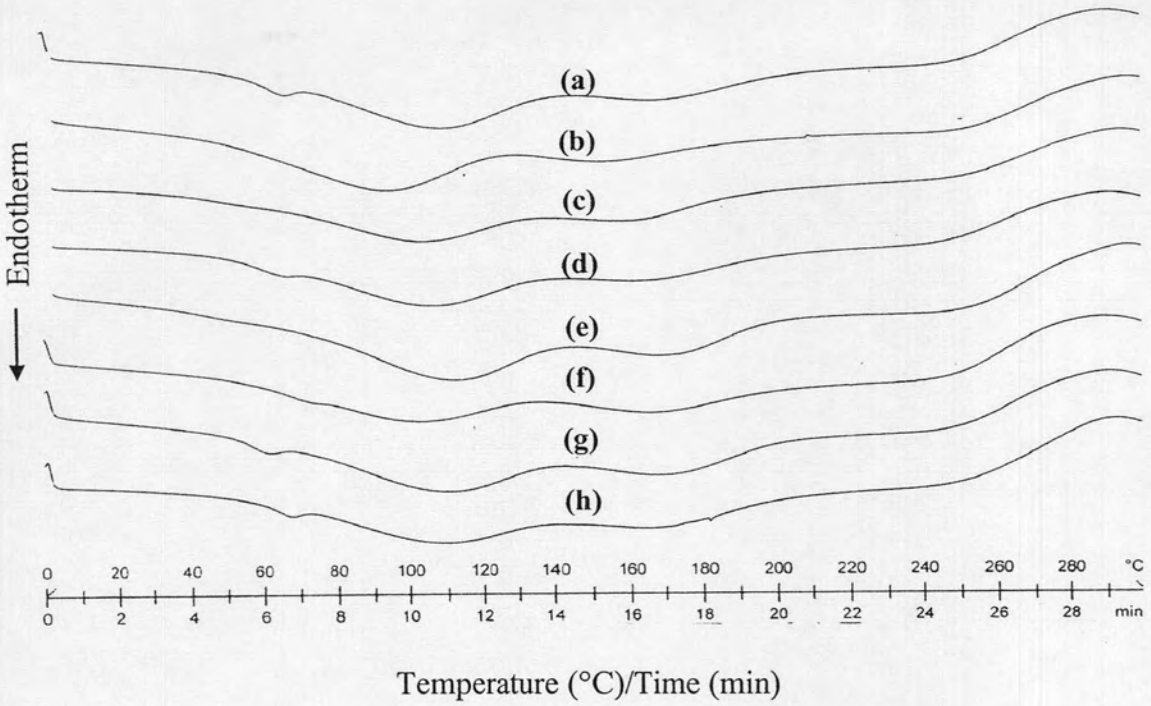

Figure 39 The DSC thermograms of F9-F16;

(a) F9

(b) F10

(c) F11

(d) F12

(e) F13

(f) F14

(g) F15

(h) F16

6. Powder X-ray diffraction

The x-ray diffractograms of standard asiaticoside, standard madecassoside, centella extract, the physical mixture of centella extract with chitosan, blank chitosan microspheres, chitosan microspheres containing centella extract (F1-16) and optimal formulation microspheres are shown in Figure 40.

The diffractograms of standard asiaticoside and madecassoside exhibited a series of intense diffraction peak, which indicative of their crystalline characteristic. The prominent peaks of x-ray diffractogram of standard asiaticoside and madecassoside were particularly observed at 12.68°, 14.24°, 15.32°, 16.56° and 12.64°, 13.36°, 13.96°, 16.24° respectively. So, the x-ray diffraction patterns of centella extract exhibited crystalline forms combined with both standard compounds.

Furthermore, the physical mixture of centella extract with chitosan as chitosan:centella extract ratio of 1:1 and 1:5 showed disappearance of centella extract diffraction peaks. This result conformed to the thermogram (Figure 37d and 37e). Chitosan microspheres showed a halo pattern diffractograms demonstrating clearly that chitosan existed in an amorphous state. The similar diffractograms were obtained with chitosan microspheres containing centella extract (F1-F16 and optimal formulation).

The x-ray diffraction study revealed that centella extract was molecularly dispersed with chitosan or/and existed in an amorphous state as a solid dispersion by spray drying. The result agreed with previous studies of chitosan microspheres containing theophylline (Asada et al., 2004) and Eudragit microspheres of itraconazole (Jung et al., 1999). The results indicated clearly that centella extract was dispersed inside the matrix of chitosan as a solid dispersion. Similar result had been reported from chitosan microspheres containing H_2 antagonist drug (He, Davis and Illum, 1999).

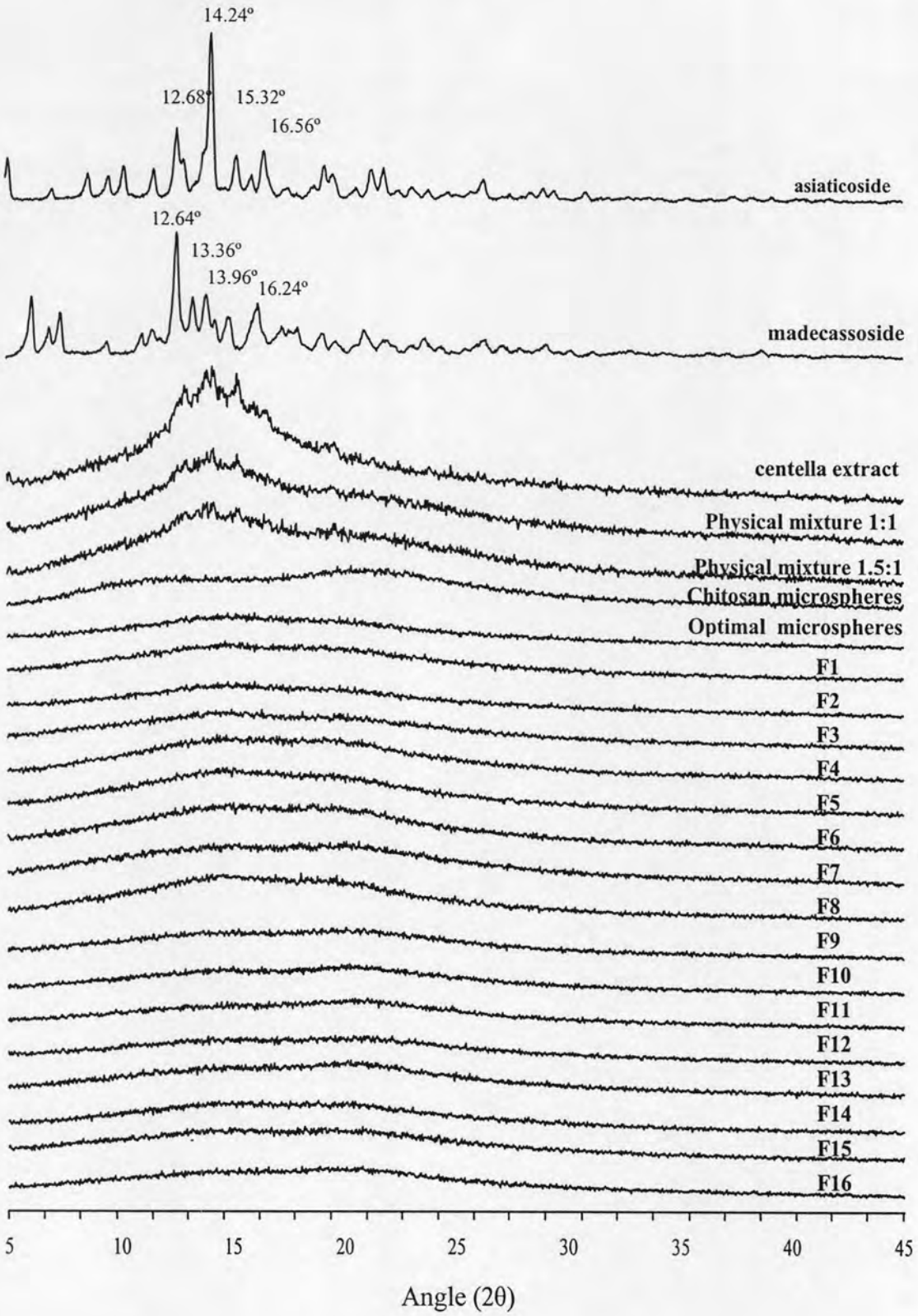

Figure 40 X-ray diffractograms of standard asiaticoside, standard madecassoside, centella extract, the physical mixture of centella extract with chitosan, chitosan microspheres, optimal microspheres and F1-16

7. %Content

Percentages content of centella extract in spray-dried microspheres of various formulations are shown in Table 18. Each formulation had good percentage of loading efficiency of above 80%. This result agreed with Hascicek, Gonul and Erk (2003) that spray drying technique was generally characterized by high drug loading efficiency.

From the result, it was observed that almost of the standard deviation of F1-8 was smaller than F9-16 and optimal formulation which implied the good uniformity of the extract distribution in F1-8. This result might be explained that in the absence of additive, Aerosil® not homogeneously dispersed within the matrix. It could be confirmed by SEM that agglomerate particles of Aerosil® was observed.

Table 18 The percentages of centella extract contents of spray-dried products (n=3)

	Formulation code	**%Content**	
		asiaticoside	**madecassoside**
Without additive	F1	97.61 ± 0.63	98.62 ± 0.70
	F2	93.97 ± 0.34	95.32 ± 1.30
	F3	94.82 ± 1.60	96.53 ± 2.55
	F4	96.79 ± 0.82	97.60 ± 0.30
	F5	94.88 ± 1.27	95.54 ± 0.81
	F6	97.13 ± 0.82	98.11 ± 0.88
	F7	93.49 ± 1.16	94.43 ± 1.32
	F8	96.12 ± 1.00	97.02 ± 1.62
With additive	F9	89.46 ± 2.46	92.47 ± 2.73
	F10	91.02 ± 1.36	94.36 ± 1.43
	F11	86.29 ± 0.94	87.25 ± 1.31
	F12	85.54 ± 2.97	88.31 ± 3.16
	F13	92.79 ± 2.68	95.09 ± 2.60
	F14	91.43 ± 1.91	94.36 ± 3.35
	F15	86.52 ± 1.26	90.88 ± 1.59
	F16	84.25 ± 1.01	86.64 ± 0.54
	Optimal microspheres	93.83 ± 1.21	96.02 ± 1.39

8. Dissolution study of the microspheres

The release profiles of asiaticoside and madecassoside from pure centella extract, chitosan microspheres F1-F16 and optimal microspheres are shown in Figure 41-46. It was found that there was the fast release during the first stage of dissolution for chitosan microspheres containing centella extract, and most of asiaticoside and madecassoside were released in a few minutes. The fast release of asiaticoside and madecassoside from chitosan microspheres prepared by the spray drying method could be due to several causes. The centella extract had been shown to be molecularly dispersed in the polymer matrix or/and dispersed in an amorphous state as demonstrated by DSC thermograms and x-ray diffractograms. This could cause a fast release of the extract. Furthermore, the microspheres formed were found to be relatively small, usually less than 10 μm in size when observation from the SEM method. When a water soluble (or even slightly water soluble) asiaticoside and madecassoside were incorporated into such microspheres, the release rate would be expected to be rapid (Giunchedi et al., 1994). The fast release of centella extract from chitosan microspheres prepared by the spray drying method could be found in a previous study that spray-dried cimetidine, famotidine and nizatidine with chitosan (He, Davis and Illum, 1999). The characteristic of fast release also occurs with some less water-soluble drugs, such as spray-dried dexamethasone with albumin (Pavenetto et al., 1994). The fast release also obtained in the dissolution of pure centella extract. It also might be that the dissolution medium in this test was 500 ml which could be sufficient to dissolve the amounts of asiaticoside and madecassoside. So, the retard dissolution was not observed.

To make an explanation for the fast release mechanism of spray-dried centella microspheres, the first order model was approached. Coefficients of determination of the relationships between log percent remained versus time (first order) of pure centella extract, chitosan microspheres F1-F16 and optimal microspheres are shown in Table 19. It was found that all formulations of microspheres and pure centella extract were fitted with first order model (for asiaticoside, R^2 = 0.9088-0.9943 and madecassoside R^2 = 0.9149-0.9998).

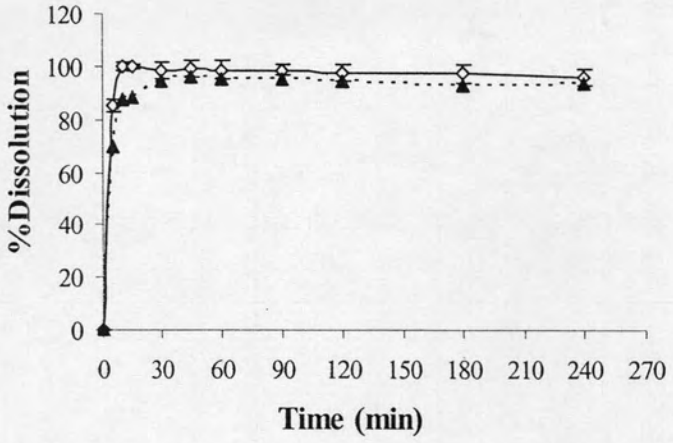

(a) Pure centella extract

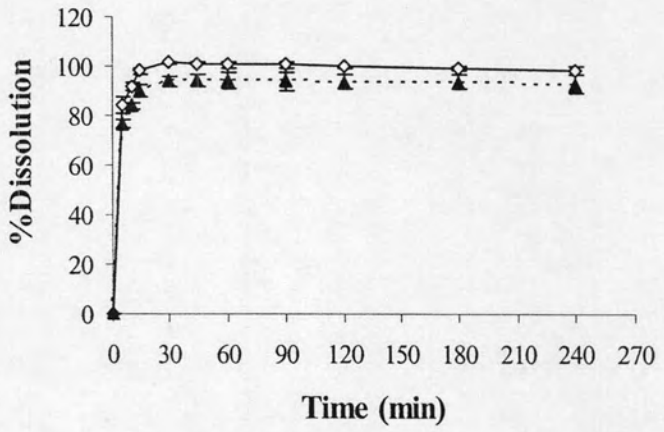

(b) F1

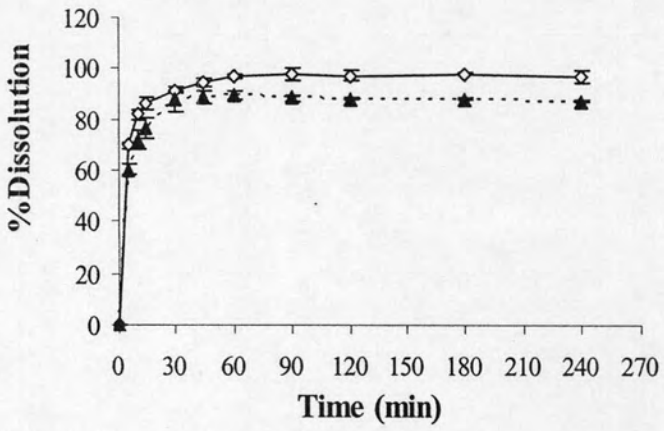

(c) F2

Figure 41 Dissolution profiles of asiaticoside (- -▲-) and madecassoside (—◇—)from;

(a) Pure centella extract

(b) F1

(c) F2

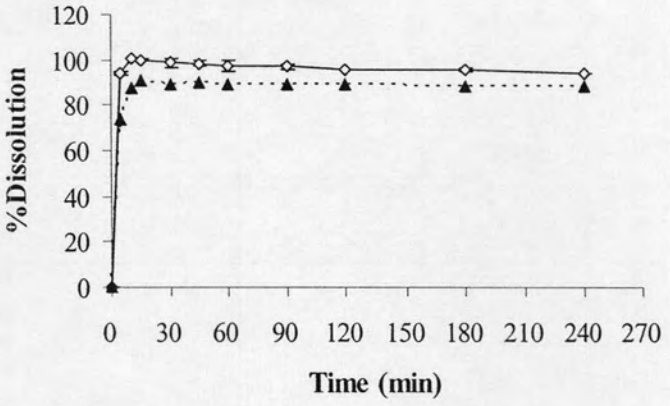

(a) F3

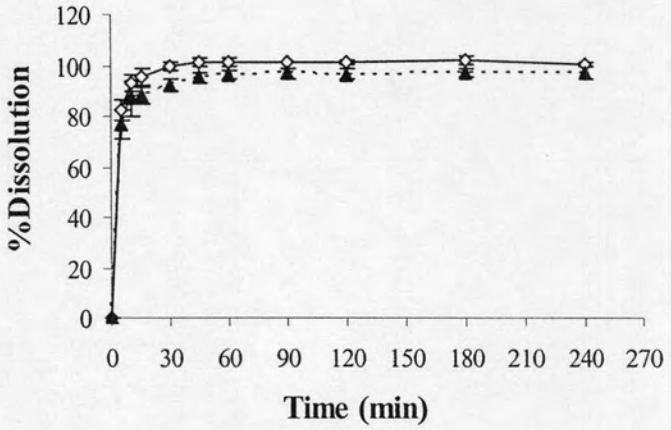

(b) F4

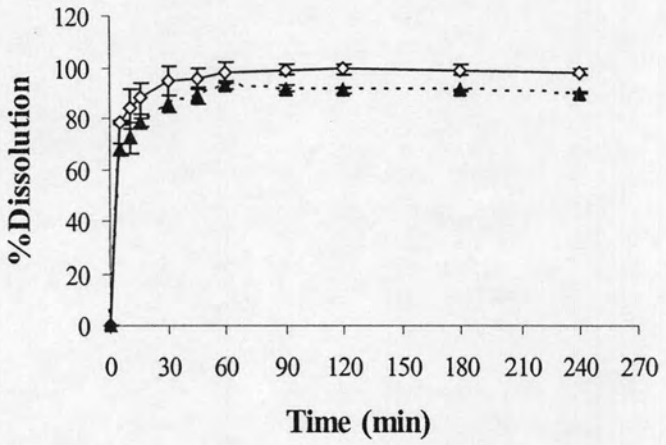

(c) F5

Figure 42 Dissolution profiles of asiaticoside (- ▲ -) and madecassoside (—◇—) from;

(a) F3

(b) F4

(c) F5

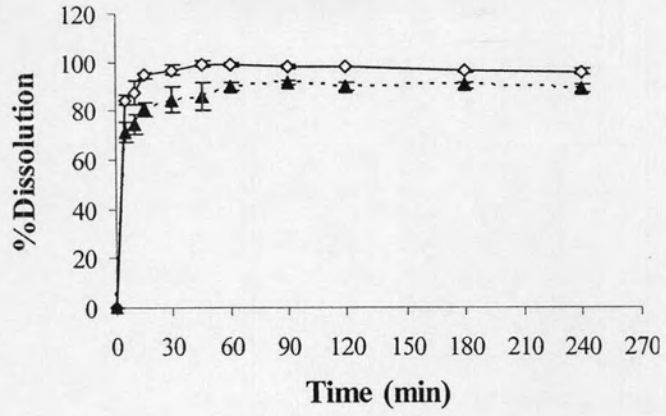

(a) F6

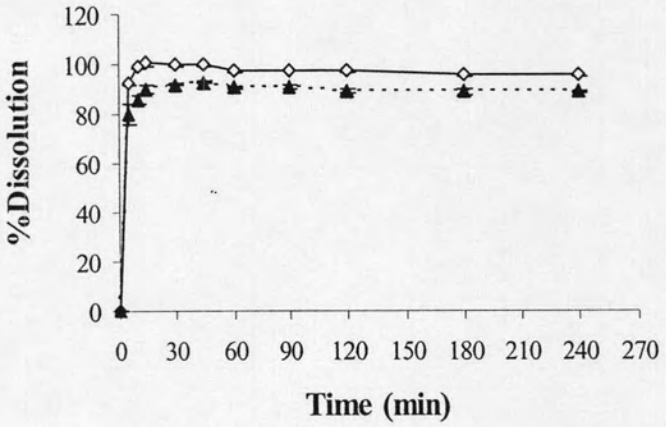

(b) F7

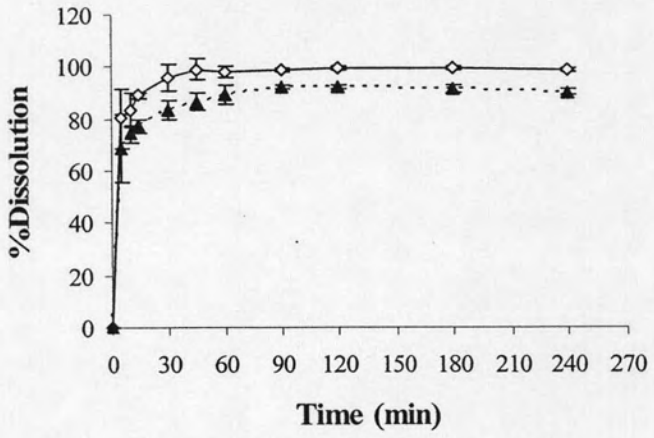

(c) F8

Figure 43 Dissolution profiles of asiaticoside (- -▲- -) and madecassoside (—◇—) from;

(a) F6

(b) F7

(c) F8

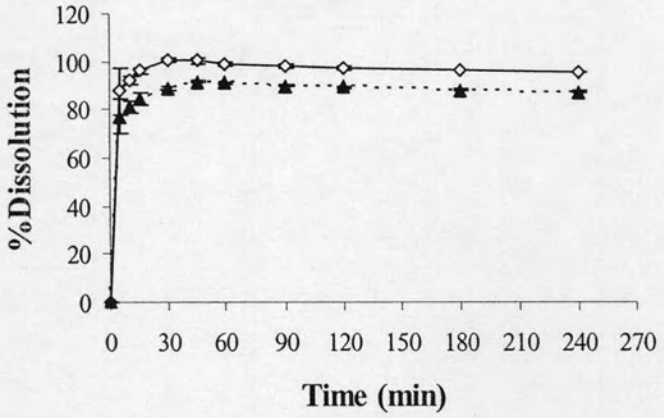

(a) F9

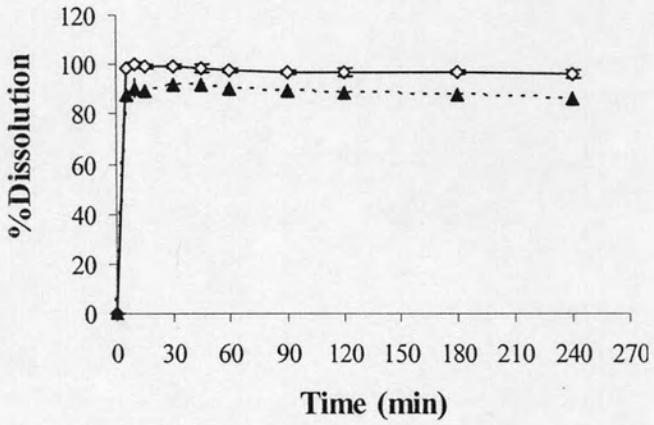

(b) F10

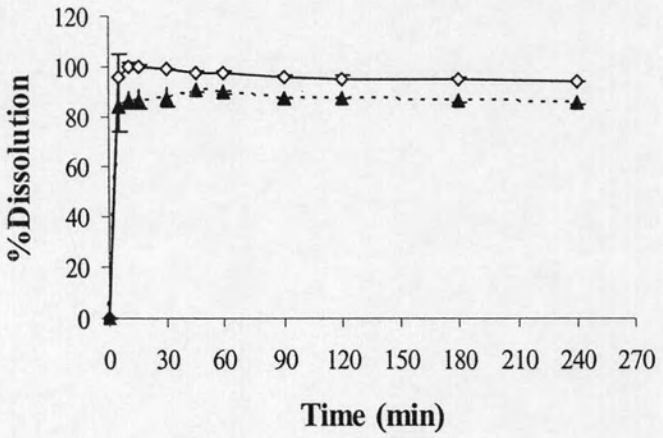

(c) F11

Figure 44 Dissolution profiles of asiaticoside (- ▲ -) and madecassoside (—◇—) from;

(a) F9

(b) F10

(c) F11

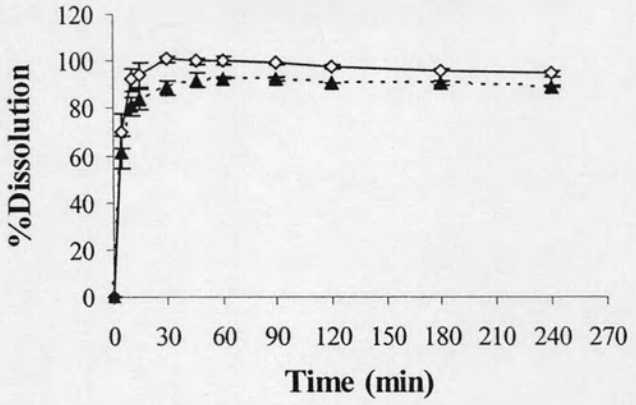

(a) F12

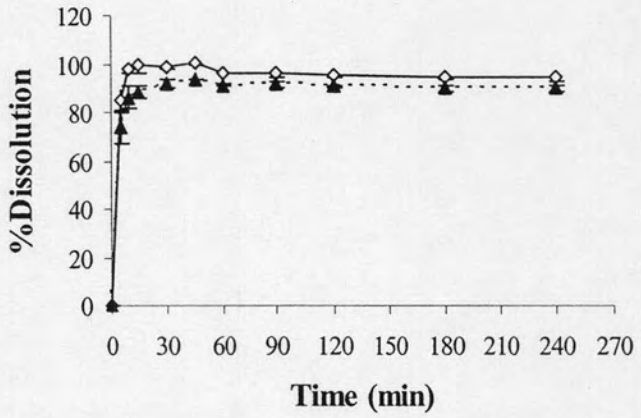

(b) F13

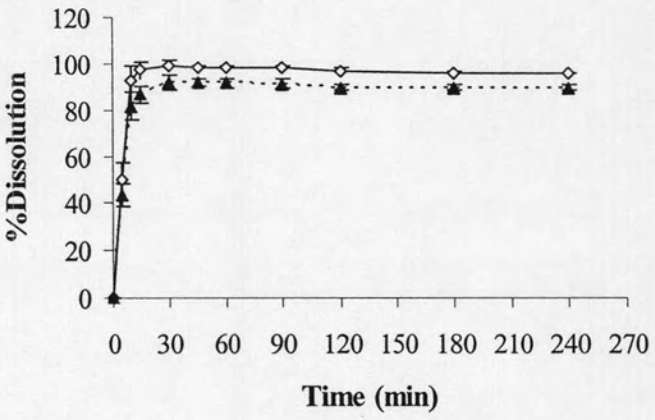

(c) F14

Figure 45 Dissolution profiles of asiaticoside (- ▲ -) and madecassoside (—◇—) from;

(a) F12

(b) F13

(c) F14

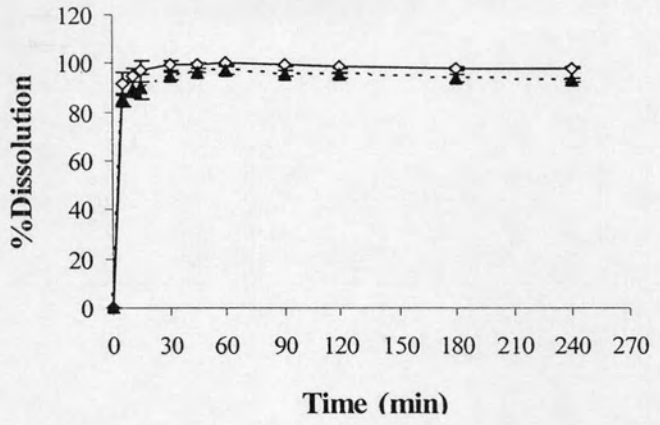

(a) F15

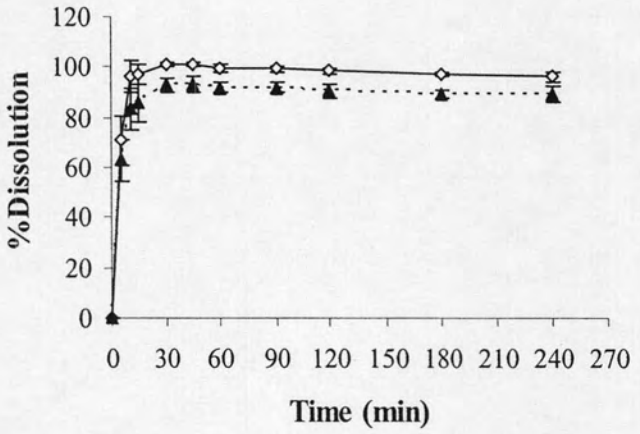

(b) F16

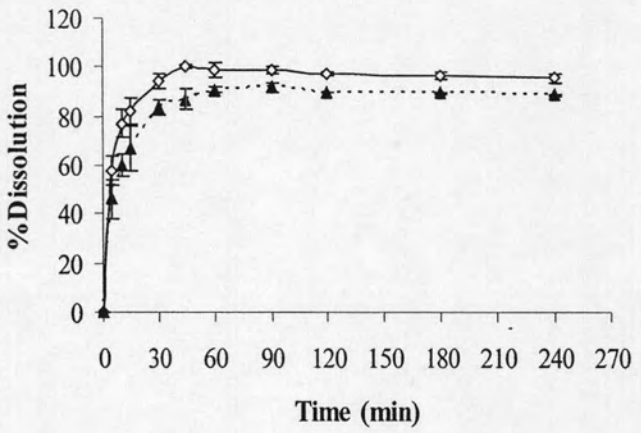

(c) optimal formulation

Figure 46 Dissolution profiles of asiaticoside (- ▲ -) and madecassoside (—◇—) from;

(a) F15

(b) F16

(c) optimal formulation

Table 19 Coefficients of determination of the relationship between log percent remained versus time (first order)

Code	Coefficients of determination (R^2)	
	asiaticoside	**madecassoside**
F1	0.9471	0.9711
F2	0.9165	0.9149
F3	0.9758	0.9838
F4	0.9520	0.9550
F5	0.9288	0.9298
F6	0.9109	0.9336
F7	0.9644	0.9988
F8	0.9156	0.9766
F9	0.9266	0.9424
F10	0.9383	0.9943
F11	0.9914	0.9997
F12	0.9088	0.9419
F13	0.9657	0.9845
F14	0.9607	0.9724
F15	0.9657	0.9869
F16	0.9781	0.9998
Optimal formulation	0.9574	0.9494
Centella extract	0.9943	0.9780

C. Characteristics of Liquid Suppositories

1. Gelation temperature of poloxamer solution

Gelation temperature is the temperature at which the liquid phase makes a transition to gel. A gelation temperature range suitable for liquid suppository would be 30-36°C. If the gelation temperature of liquid suppository was lower than 30°C, gelation occurs at room temperature leading to difficultly in manufacturing, handling and administering. If the gelation temperature of liquid suppository was higher than 36°C, the suppository still stays solution at body temperature, resulting in leakage from the anus. Therefore, liquid suppository must have the suitable gelation temperature, range from 30-36°C that is to be a liquid from at room temperature and to form a gel phase in the rectum.

The apparatus for gelation temperature measurement in this investigation was assembled in the laboratory of the Department of Pharmacy (Figure 11). The apparatus was adapted from the method described by Choi et al. (1998). The measurement obtained from the apparatus demonstrated a high precision. From Table 20 the standard deviations were found lower than ±1.0°C. As reported in Table 20, this study found that the poloxamer solution less than 17% w/w of P407 did not from a gel over the temperature ranges tested (up to 50°C), and that increasing concentration of P407 by an increment of 2-3%, decreased its gelation temperature. The gelation temperatures of poloxamer solutions containing 17–30% w/w of P407 alone were 26.4±0.19 to14.5±0.08°C by beginning concentration that formed gel at room temperature was 20%w/w. The results conformed to the data (Rowe, Sheskey and Weller, 2003) that P407 geled at a concentration 20%w/w at 25°C. The solution behaved as a mobile viscous liquid at temperature below 25°C.

On the other hand, P188 in the tested concentration were 20-30%, they failed to give the suitable range of gelation temperature, where all the recorded temperature values were >50°C and a gelation started to be observed at 52.8±0.23 °C with a 30% w/w of P188. This meaned that increasing the P188 and P407 concentrations decreased the gelation temperature. This indicated that P407 or P188 alone could not provide the suitable gelation temperature.

Table 20 Gelation temperatures of poloxamer solutions (n=5)

Code	Poloxamer	Concentration (%w/w)	Gelation temperature (°C)
	P407		
1		10	>50
2		15	>50
3		17	26.4 ± 0.19
4		20	22.3 ± 0.15
5		23	19.7 ± 0.13
6		25	18.1 ± 0.20
7		27	16.7 ± 0.15
8		30	14.5 ± 0.08
	P188		
9		20	>50
10		25	>50
11		30	>50 (52.8 ± 0.23)
	P407/P188		
12		15/10	44.2 ± 0.21
13		15/15	40.5 ± 0.25
14		16/4	39.9 ± 0.55
15		16/8	40.6 ± 0.33
16		17/5	39.6 ± 0.24
17		17/10	41.8 ± 0.19
18		18/4	33.6 ± 0.15
19		20/5	32.1 ± 0.20
20		20/10	33.6 ± 0.15
21		25/5	21.3 ± 0.11
22		25/10	27.5 ± 0.26

A modulation of the gelation temperature to reach the desired range (30-36°C) could be achieved through the use of a combination of the two poloxamer types. It was also noticed that, with all the concentrations of P188 (4-10% w/w), mixtures containing lower percentage of P407. These preparations were gelled at a higher temperature than formulation containing the higher percentage. Similar results were reported from the study of *in situ* gelling and mucoadhesive mebeverine hydrochloride solution (El-Hady et al., 2003). This revealed that P407 was the main polymer

determining the gelation temperature of the solution because its concentration resulted to gel, which was less than that of the other members of the poloxamer series and might be explained on the basis of its higher molecular weight of P407 (average Mw 12196) compared to that of P188 (average Mw 8270) and its higher amount in the formulation.

The w/w percentage ratios P407/P188 with a suitable gelation temperature of 32.1±0.20, 33.6±0.15 and 33.6±0.15°C were 20/5, 20/10 and 18/4% w/w, respectively. These suitable formulations were selected as the systems of choice for the liquid suppository since they might give flexibility in formulation with other components. The results are shown in Table 20.

Poloxamer solutions were known to exhibit the thermoreversible gelation, the thermoreversibility of poloxamers could be explained on the basis that they were more soluble in cold water than hot water. The gelation mechanism of poloxamer solutions had been investigated extensively, but was stilled being debated. Being the surfactant in nature, the temperature-dependent gelation of poloxamer solutions could be explained as being a change in their micellar properties.

Micelle formation occurs at the critical micellization temperature as a result of PPO block dehydration (Bohorquez et al., 1999). With raising the temperature, at a definite point, micelles come into contact and no longer move. In addition, the formation of highly ordered structures, such as cubic crystalline phase, had been proposed as the driving force for gel formation (Mortensen and Pederson, 1992), but this hypothesis had been questioned. Thus packing of micelles and micelle entanglements might be possible mechanisms of poloxamer solution gelation with increased of temperature (Cabana, Ait-Kadi and Juhasz, 1997)

2. Gel strength of poloxamer solution

In the development of liquid suppository, the gel strength is important in finding the condition which allows the easy insertion of the suppositories and no leakage from the anus. It had been previously reported that the optimal *in situ* gelling poloxamer solution must had suitable gel strength, in the range of 10 to 50 seconds (Choi et al., 1998).

The apparatus used to determine gel strength in this investigation was designed and adapted from Choi et al. (1998). The apparatus gave a measurement with low standard deviations (Table 21). From Table 20, the three formulations composed of

20/5, 20/10 and 18/4%w/w of P407/P188 were selected to the gel strength measurement, since they gave the suitable range of gelation temperature. The measured gel strength of the former poloxamer solution is shown in Table 21. The gel strength of 18/4% w/w was 46.8 seconds while these of 20/5, 20/10% w/w were higher than 50 seconds. So, the formulation composed of 18/4%w/w of P407/P188 were selected to study for the setting time measurement, since it gave the suitable range of gel strength.

The results obtained might be attribute to the higher total concentrations of combined poloxamers that gave the higher gel strengths. The formulas P407/P188 of 20/5, 20/10 and 18/4%w/w had total poloxamer concentrations of 25, 30 and 22%w/w, respectively.

Table 21 Gel strengths of poloxamer solutions (n=5)

P407/P188 (% w/w)	Gel strength (s)
20/5	>50
20/10	>50
18/4	46.8 ± 1.30

3. Setting time of poloxamer solution

Setting time is the time at which the liquid phase makes a transition to gel. If the setting time of liquid suppository is a little time, instantly gelation occurs in the rectum, resulting in no leakage from the anus. The poloxamer solution composed of 18/4% w/w with optimal physical parameters including a gelation temperature (33.6±0.15 °C) and gel strength (46.8±1.30 seconds) was selected to study for the setting time. The poloxamer solution of 18/4% w/w gave the setting time within 30 seconds. This value explained that liquid suppository could be gel immediately at body temperature.

Since chitosan microspheres containing centella extract were the active material of the poloxamer base suppository, the effect of microspheres on the physical characteristics of the suppositories should be studied. In the experiments, the amount of microspheres was fixed at asiaticoside equivalent to 8 mg/dose. The results showed that the gelation temperature of descreased to 32.5±0.15 °C but gel strength increased

to 49.7±1.53 seconds (Table 22). This might be due to possible interaction of microsphere components with poloxamer.

Table 22 Effect of centella microspheres on the physical properties of poloxamer base

Physical properties ± SD	P407/P188 (18/4%w/w)	
	without microspheres	added microspheres
Gelation temperature (° C)	33.6 ± 0.15	32.5 ± 0.15
Gel strength (s)	46.8 ± 1.30	49.7 ± 1.53
Setting time (s)	30 ± 0.00	30 ± 0.00

From these finding in our study, it suggested that the poloxamer solution composed of 18/4%w/w of P407/P188 was the optimal system which had the gelation temperature, gel strength and setting time suitable for liquid suppository.

Thus it was selected to be a base for liquid suppository for in vitro release study to verify the release characteristics of *in situ* gelling suppository, two types of conventional suppositories, hydrophilic and lipophilic bases were compared.

4. *In vitro* release of asiaticoside and madecassoside from suppositories

Since an official in vitro release method was not available for the test of drug release from rectal dosage form, in vitro release of the active ingredients from rectal suppository was thus, carried out using the USP paddle dissolution apparatus.

In this test, conventional suppositories (hydrophilic and lipophilic) and poloxamer liquid suppository, added with either pure centella extract or centella extract spray-dried with chitosan were investigated. The analytical method, which employed in this investigation, was the HPLC method as previously described. Figure 47 is shown each type of suppositories in this experiment.

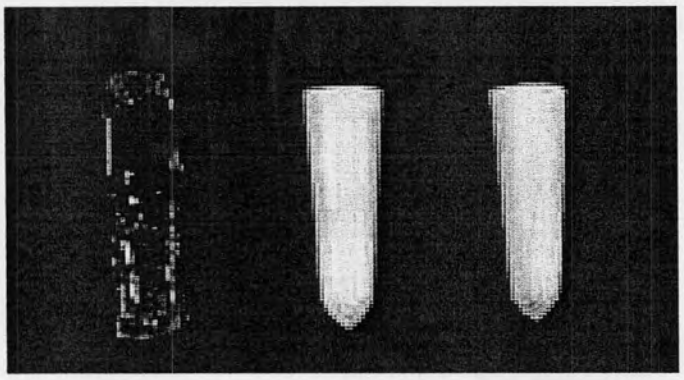

(a) (b) (c)

Figure 47 The suppositories for in vitro release analyse;

(a) centella liquid suppository in sugar tube

(b) centella hydrophilic suppository (PEGs, water soluble base)

(c) centella lipophilic suppository (Suppocire®AM, oleaginous base)

In vitro dissolution profiles from the three different suppositories were dependent on the types of base and forms of extract (pure centella extract or centella extract spray-dried with chitosan). The release data and profiles of asiaticoside and madecassoside from the different formulations with the variation of base suppositories (Suppocire®AM, PEGs and poloxamer), are illustrated in Tables 23-24 and Figures 48-49 respectively.

The hydrophilic conventional suppository and liquid suppository decreased gradually in size during the dissolution test but the lipophilic suppository melted and spread due to the temperature of the medium and the agitation.

Table 23 Release of asiaticoside and madecassoside from pure centella extract with the variation of base suppositories (n=3)

Time (min)	%Release ± SD					
	Active: pure centella extract					
	Suppocire®AM		PEGs		Poloxamer	
	asiaticoside	madecassoside	asiaticoside	madecassoside	asiaticoside	madecassoside
0	0.00	0.00	0.00	0.00	0.00	0.00
10	31.25±6.02	40.52±7.86	48.35±7.45	42.88±8.82	41.85±3.81	51.43±1.41
20	47.99±6.31	60.35±0.91	75.59±2.84	92.61±1.41	62.54±3.09	76.65±1.40
30	63.09±1.49	77.04±1.51	83.58±2.65	96.44±4.71	75.16±3.16	92.05±0.89
45	76.19±2.19	89.72±2.72	86.55±2.52	98.30±1.20	81.15±1.27	95.67±2.65
60	89.01±0.33	98.94±0.57	86.63±0.49	95.62±1.89	86.93±1.68	96.36±2.22
120	87.73±0.36	98.97±1.88	85.31±0.47	94.48±1.29	87.68±0.64	97.38±2.58
180	86.87±0.81	98.02±1.09	85.23±0.54	95.43±0.69	86.83±0.89	96.98±1.66
240	86.36±0.35	96.19±0.96	84.65±0.37	93.73±1.80	86.91±0.53	97.61±0.54

Table 24 Release of asiaticoside and madecassoside from spray-dried centella extract with chitosan with the variation of base suppositories (n=3)

Time (min)	%Release ± SD					
	Active: spray-dried centella extract with chitosan					
	Suppocire®AM		PEGs		Poloxamer	
	asiaticoside	madecassoside	asiaticoside	madecassoside	asiaticoside	madecassoside
0	0.00	0.00	0.00	0.00	0.00	0.00
10	54.75±3.11	76.64±2.34	27.14±2.28	35.35±1.93	33.60±0.89	47.52±2.25
20	80.79±0.81	91.54±1.07	67.86±1.01	79.57±1.13	50.90±1.22	65.34±1.32
30	88.67±0.24	96.27±0.78	87.70±1.95	95.61±5.40	63.02±1.23	83.80±2.14
45	87.74±0.89	97.89±0.30	90.45±1.36	97.15±3.76	80.78±2.01	95.38±1.31
60	86.42±0.65	96.01±1.74	89.35±0.61	97.90±0.95	83.11±1.23	98.66±1.69
120	85.65±0.44	95.71±0.45	88.64±0.94	98.56±0.46	84.87±1.01	99.82±0.96
180	85.19±0.40	93.16±1.77	87.92±0.87	97.71±0.52	85.32±1.67	100.52±0.54
240	84.63±0.32	93.73±0.92	87.52±0.86	96.08±1.74	86.58±1.68	100.18±0.65

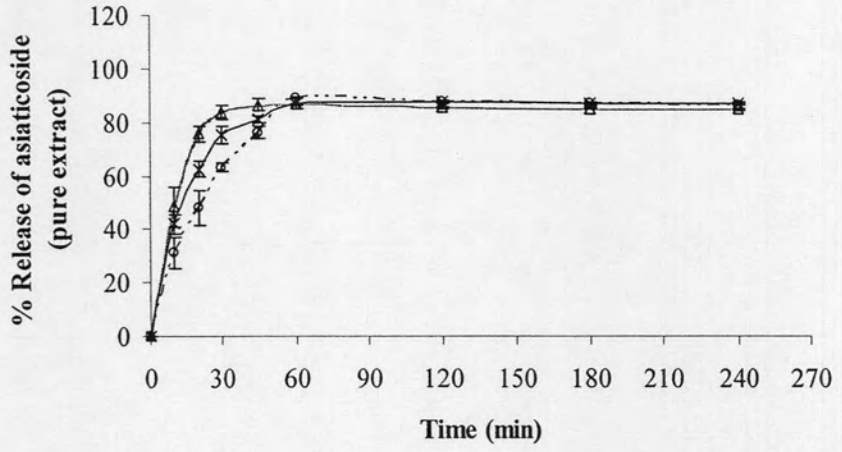

(a) asiaticoside

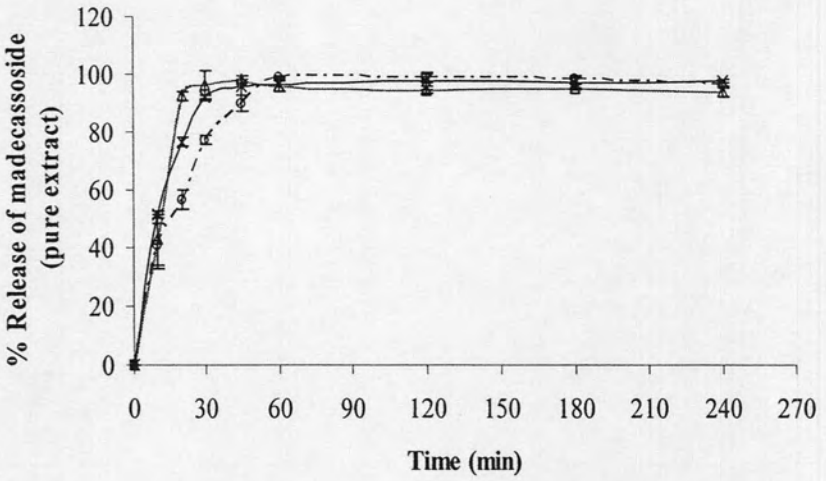

(b) madecassoside

Figure 48 Release profiles of asiaticoside and madecassoside from pure centella extract in suppositories prepared with; Suppocire®AM (—·⊙—·—), PEGs (—△—) and poloxamer (—×—);

(a) asiaticoside

(b) madecassoside

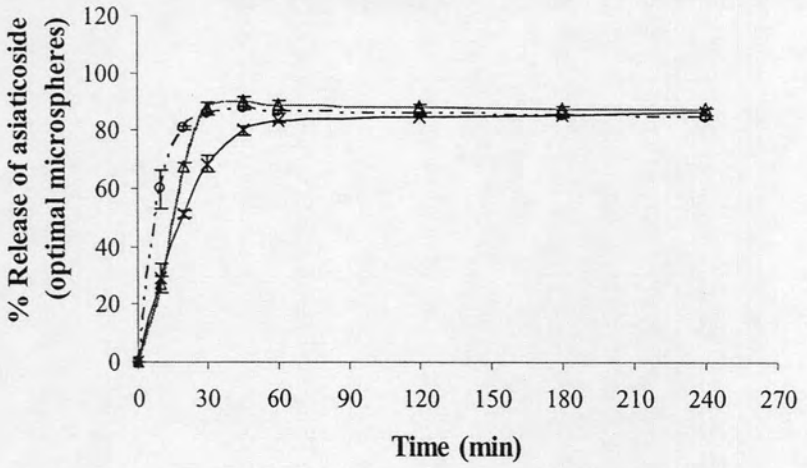

(a) asiaticoside

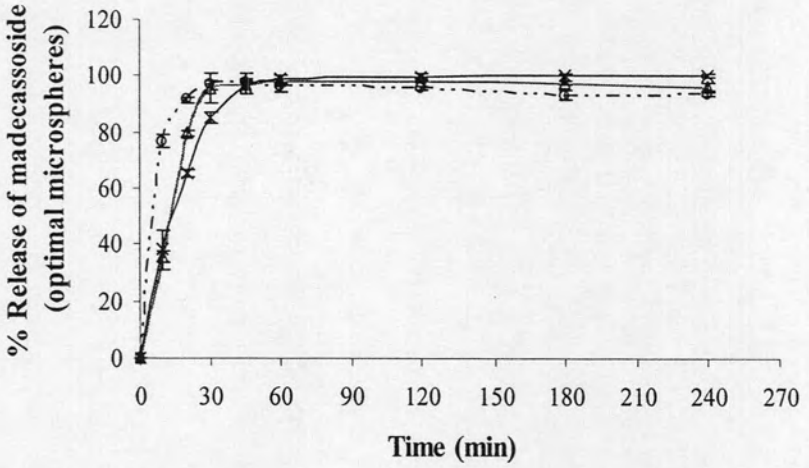

(b) madecassoside

Figure 49 Release profiles of asiaticoside and madecassoside from spray-dried centella extract with chitosan in suppositories prepared with; Suppocire®AM (—·⊙—·), PEGs (—△—) and poloxamer (—×—);

(a) asiaticoside

(b) madecassoside

The release results, $T_{80\%}$, showed that the lipophilic base suppository (Suppocire®AM) composed of pure centella extract, released more than 80% of asiaticoside and madecassoside within 60 minutes. However, the hydrophilic base suppository (PEGs) and liquid suppository (poloxamer) gave fasten release as compared to fatty base. The percentages of asiaticoside and madecassoside were dissolved more than 80% within 30 and 45 minutes for PEGs and poloxamer base, respectively. On the other hand, lipophilic base suppository composed of centella microspheres, released more than 80% of asiaticoside and madecassoside within 20 minutes. The dissolution time for more than 80% of asiaticoside and madecassoside were within 30 and 45 minutes for PEGs and poloxamer base, respectively (Table 25), which revealed slower release as compared to the fatty base.

It might be explained on the basis that Suppocire®AM was lipophilic suppository, whereas spray-dried centella with chitosan was much water soluble than pure centella extract. So, they provided a general summary of the relationship of drug release which a water soluble drug in an oily base showed rapid release and an oil soluble drug with water miscible base showed moderate release.

Table 25 $T_{80\%}$ of asiaticoside and madecassoside depended on the types of base and forms of active

Bases	**Forms of active**	$T_{80\%}$ **(min)**	
		asiaticoside	**madecassoside**
Suppocire® AM	pure centella extract	60	45
	spray-dried centella microspheres	20	20
PEGs	pure centella extract	30	20
	spray-dried centella microspheres	30	30
Poloxamer	pure centella extract	45	30
	spray-dried centella microspheres	45	30

The release mechanisms of asiaticoside and madecassoside released from several formulations of suppositories were determined by finding the best fit of the dissolution data (drug-released fraction versus time) to distinct models: first-order and Higuchi model (Table 26a and 26b).

Table 26 Fitting results of the asiaticoside and madecassoside release data from all suppositories

a) First order kinetics from Suppocire® AM and PEGs bases

Formulations			First-order	
Types of Base	**Types of extract**	**Active ingredients**	k_1 (h^{-1})	R^2
Suppocire® AM	Pure centella extract	asiaticoside	0.825	0.9980
		madecassoside	1.307	0.9978
	Spray-dried centella extract with chitosan	asiaticoside	1.926	0.9908
		madecassoside	2.836	0.9828
PEGs	Pure centella extract	asiaticoside	1.607	0.9859
		madecassoside	3.140	0.9479
	Spray-dried centella extract with chitosan	asiaticoside	1.851	0.9582
		madecassoside	2.743	0.9473

b) Higuchi model from poloxamer base

Formulations			Higuchi model	
Types of Base	**Types of extract**	**Active ingredients**	$k_H \times 10^{-2}$ ($\%h^{-1/2}$)	R^2
Poloxamer	Pure centella extract	asiaticoside	1.070	0.9989
		madecassoside	1.311	0.9990
	Spray-dried centella extract with chitosan	asiaticoside	0.890	0.9977
		madecassoside	1.169	0.9986

Figures 48-49 demonstrated the release profiles of asiaticoside and madecassoside from all formulations. In this study, it was found that the releases from PEGs and Suppocire®AM base containing both pure centella extract and spray-dried with chitosan were fitted with first order model (R^2 = 0.9473-0.9980) (Table 26a). The mechanism of first order model from Suppocire®AM released was previously reported by Samy et al. (2000) that studied availability of allopurinol in suppositories dosage form.

The releases from poloxamer containing both pure centella extract and spray-dried with chitosan were fitted with Higuchi model (R^2 = 0.9977-0.9990) (Table 26b). The release mechanism of centella extract from poloxamer base that fitted the Higuchi model was consistent with Kim et al. (1998) and El-Kamel and El-Khatib (2006) that studied mucoadhesive liquid suppository containing acetaminophen and carbamazepine, respectively. However, the result did not agree with El-Hady et al. (2003) that studied mucoadhesive liquid suppository containing mebeverine hydrochloride which showed release profile with zero order release kinetic. From poloxamer liquid suppository bases, it suggested that asiaticoside and madecassoside might release from these formulations by Fickian diffusion through extramicellar aqueous channels of the gel matrix which meaned the outer layer of poloxamer cross-linking system (poloxamer micelle) (Kim et al., 1998). As the poloxamer gels were considered to consist of large populations of micelles in aqueous phase. So, the incorporated solute might be released by diffusion through aqueous extramicellar channels of the gel matrix. The size of the aqueous channels, the arrangement of the drug between the micelles and the aqueous phase, and the microviscosity of the extramicellar fluid could affect the release of the drug (Chen- Chow and Frank, 1981; Rassing and Attwood, 1983). Additionally the PEGs base suppository had higher dissolution rates than poloxamer base suppository. The result suggested that PEGs were soluble in the dissolution medium, while poloxamer was not soluble but gelled (Choi, Oh and Kim, 1998). The poloxamer gel structure was more closely packed and act as a resistant barrier for drug release. Furthermore, the release rate was dependent on how fast the PEGs base dissolved. Usually, dissolution of PEGs was dependent on their molecular weights. Thus, PEGs base in this study with higher portion of low molecular weight component could dissolve rapidly.

D. Stability Study of Chitosan Microspheres Containing Centella Extract

The stability study of centella extract in chitosan microspheres was performed by triplicate samples of optimal formulation. They individually packed in glass vials which tightly sealed with rubber closures and aluminum caps and stored at 40°C, 75% RH for three months. At the initial time, first, second and third month, the microspheres were sampled and assayed for the remaining asiaticoside and madecassoside contents. The physicochemical properties and the amounts of asiaticoside and madecassoside of microspheres in stability test were determined using differential scanning calorimetry (DSC), powder x-ray diffraction and quantitatively analyzed with high performance liquid chromatography (HPLC), respectively.

1. Physicochemical stability study

1.1 Differential scanning calorimetry (DSC)

The DSC thermogram change was used as an effective tool to investigate the physicochemical stability of the microspheres containing centella extract. As the results of the DSC thermograms of the optimal formulation, no change in DSC thermograms between three months of stability study as compared to that at the initial was observed. These results indicated that the optimal formulation did not change in physicochemical properties after the stress condition for 3 months (Figure 50). The centella extract showed the stable existence in chitosan matrix as an amorphous state.

1.2 Powder x-ray diffraction

The powder x-ray diffraction study was carried out to elevating crystallinity change of the compound. As the results of the diffractograms of the optimal formulation, no change in diffractograms between three months of stability study as compared to that at the initial time was observed as well. These results were conformed the DSC study that the optimal formulation did not change in physicochemical properties after the stress condition for 3 months (Figure 51). All diffractograms demonstrated no diffraction peak that corresponding to crystallinity occurred.

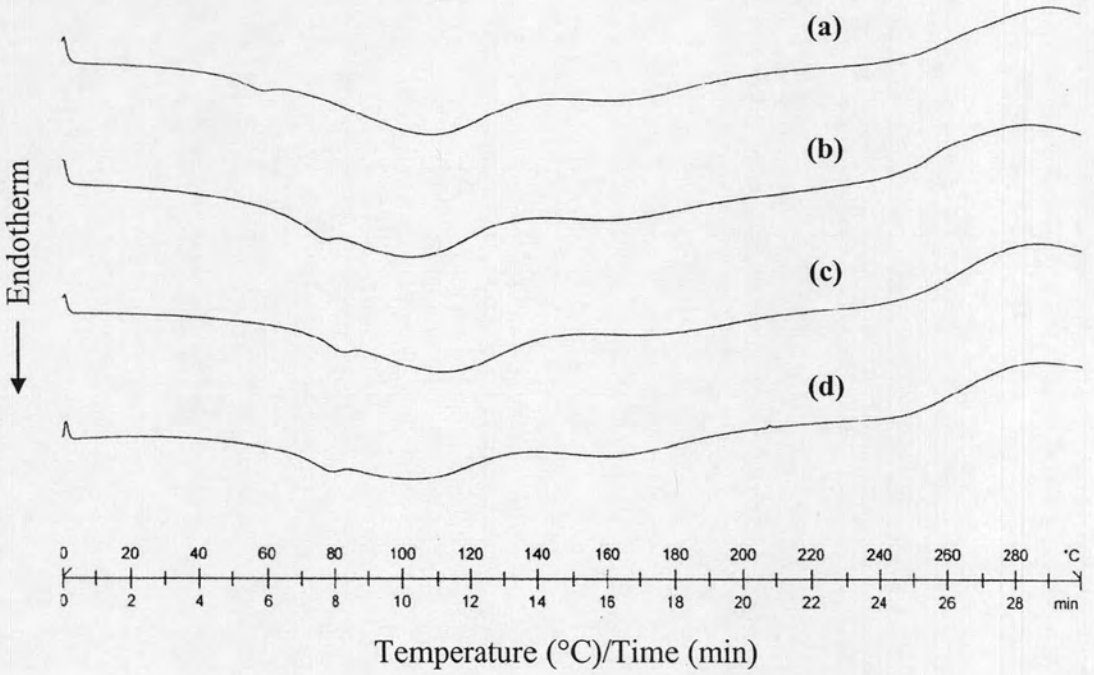

Figure 50 DSC thermograms of optimal formulation microspheres after stress condition (40° C, 75% RH);

(a) at initial time

(b) at first month

(c) at second month

(d) at third month

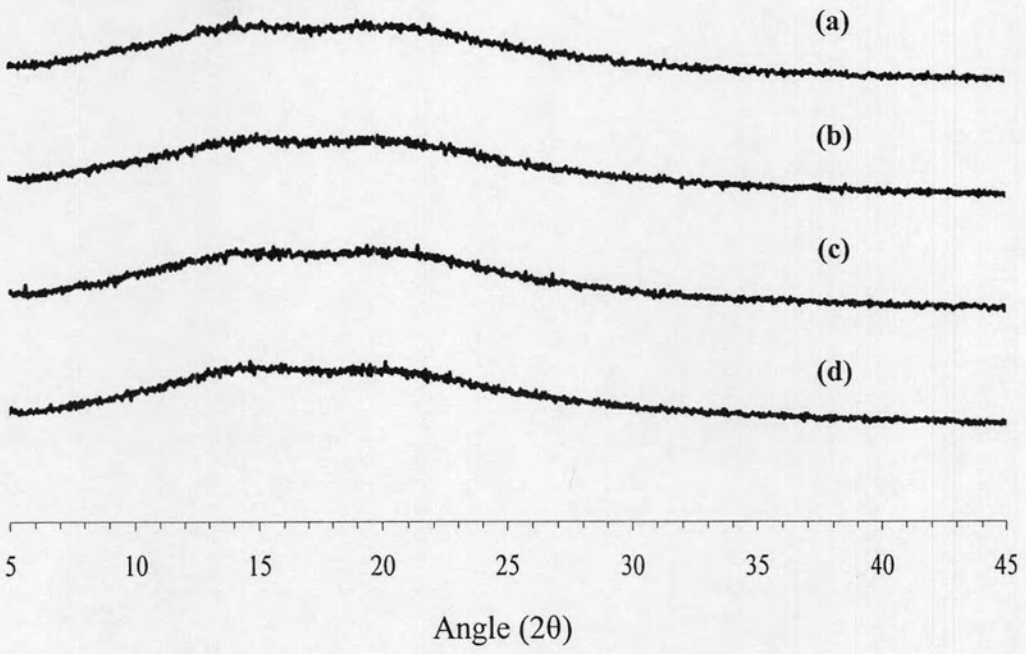

Figure 51 X-ray diffractograms of optimal formulation microspheres after stress condition (40° C, 75% RH);

(a) at initial time

(b) at first month

(c) at second month

(d) at third month

2. Chemical stability study

The amounts of asiaticoside and madecassoside in microspheres were assayed by HPLC method at 0, 1, 2 and 3 month period. The analytical method, which employed in this investigation, was the HPLC method as previously described. In addition, the percentage lossed of asiaticoside and madecassoside and percentages labeled amount after the exposure to heat and high humidity (40±2 °C, 75±5% RH) at each time interval and the end of storage were also calculated. The previous study had been reported that asiaticoside might be degraded by peroxide, acid and alkaline agents. Asiaticoside was degraded by oxidation mechanism to obtain other compounds while was hydrolyzed by hydronium/hydroxide ion to obtain asiatic acid and sugar moiety, glucose and rhamnose (Hengsawas, 2004). The mechanisms of hydrolysis are proposed in Figures 52-53.

From the result, the percentage loss of asiaticoside and madecassoside during 3 month periods were 4.91 and 4.54%, respectively (Table 27).

Table 27 Percentages labeled amount of asiaticoside and madecassoside in optimal microspheres in stability test

Periods	%Labeled amount ± SD	
	asiaticoside	**madecassoside**
Initial	93.83 ± 2.20	96.02 ± 2.50
1st month	91.89 ± 0.28	92.10 ± 0.71
2nd month	90.71 ± 1.14	92.14 ± 0.39
3rd month	89.22 ± 0.85	91.66 ± 1.04
% loss	4.91	4.54

* $\%loss = \frac{\text{initial - final\% labeled amount}}{\text{initial\% labeled amount}} \times 100$

As the results, centella microspheres appeared to be stable during 3 month periods due to its percentage loss of asiaticoside and madecassoside were less than 10% of the initial value (Cartensen, 1990).

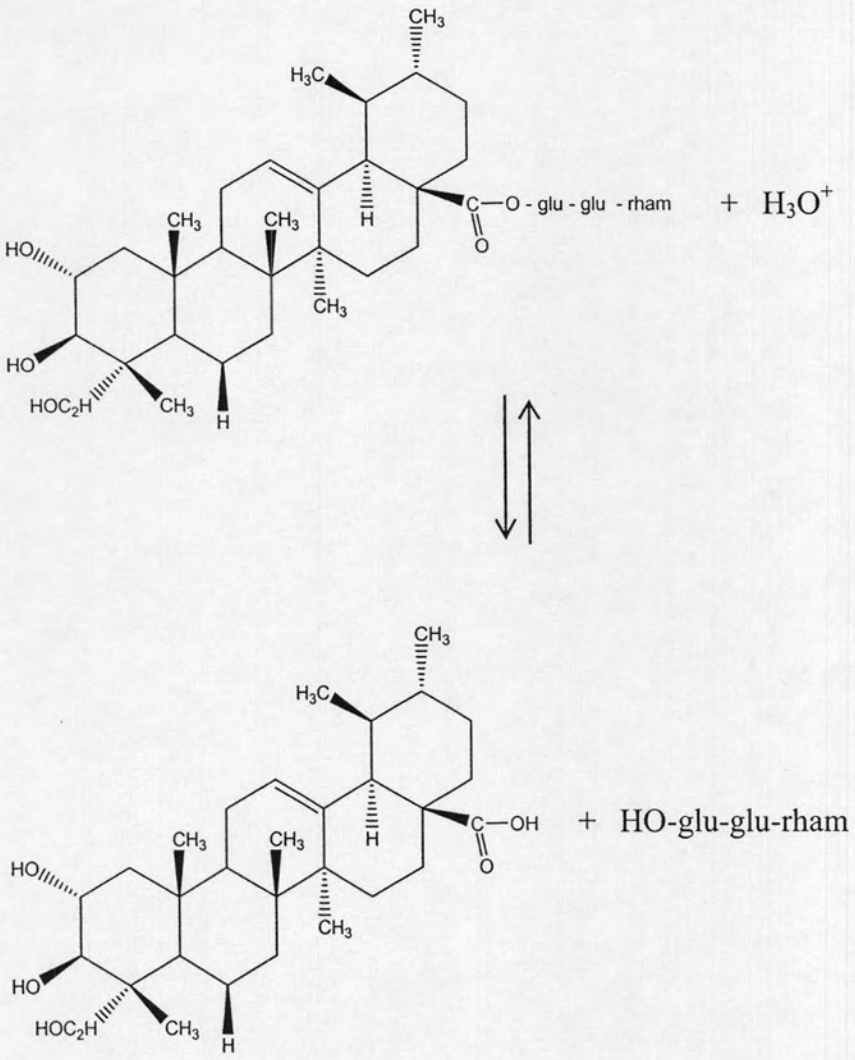

Figure 52 Hydrolysis of asiaticoside by hydronium ion

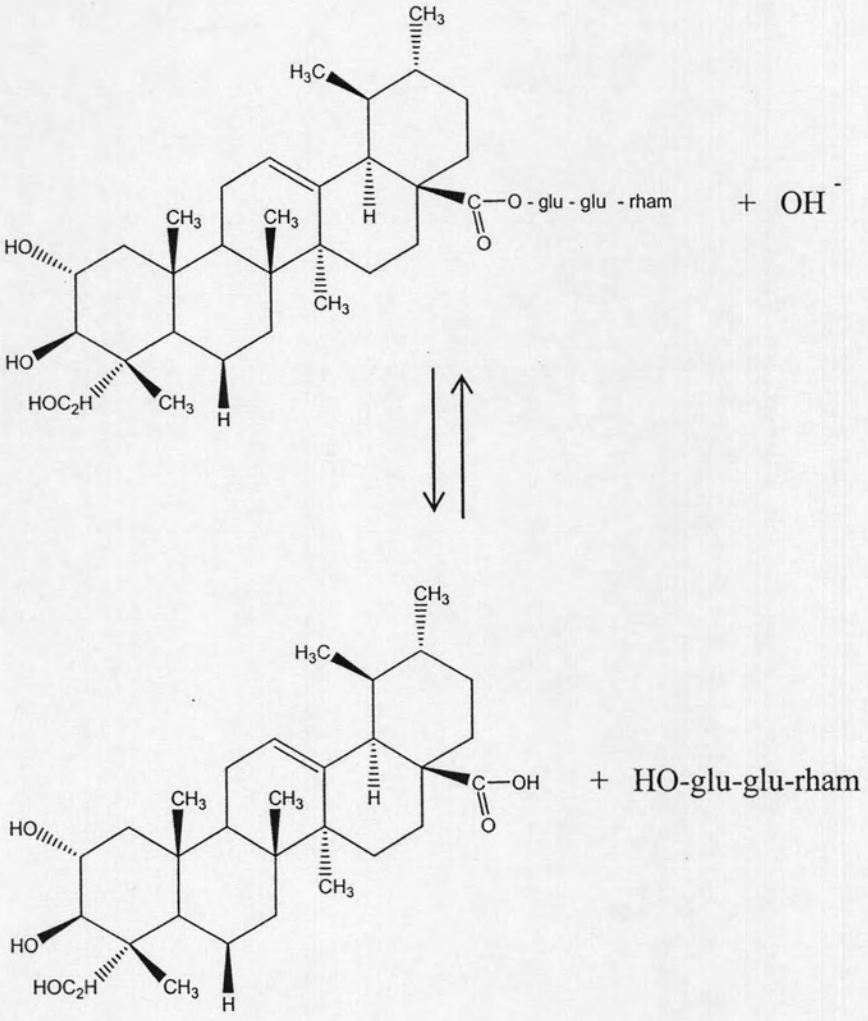

Figure 53 Hydrolysis of asiaticoside by hydroxide ion